

Long-term preservation of Hadean protocrust in Earth's mantle

Jonas Tusch^{1,1}, Elis Hoffmann^{2,2}, Eric Hasenstab^{1,1}, Carsten Münker^{1,1}, Mario Fischer-Gödde³, and Chris S. Marien¹

¹Universität zu Köln

²Freie Universität Berlin

³University of Cologne

November 30, 2022

Abstract

With plate tectonics operating on Earth, the preservation potential for mantle reservoirs from the Hadean Eon (>4.0 Ga) has been regarded as very small. The quest for such early remnants has been spurred by the observation that many Archean rocks exhibit excesses of ^{182}W , the decay product of short-lived ^{182}Hf . However, it remains speculative, if Archean ^{182}W anomalies and also ^{182}W deficits found in many young ocean island basalts (OIBs) mirror primordial Hadean mantle differentiation or just variable contributions from older meteorite building blocks delivered to the growing Earth. Here, we present a high-precision ^{182}W isotope dataset for 3.22-3.55 Ga old rocks from the Kaapvaal Craton, southern Africa. In expanding previous work, our study reveals widespread ^{182}W deficits in different rock units from the Kaapvaal Craton and also the very first discovery of a negative co-variation between short-lived ^{182}W and long-lived ^{176}Hf - ^{143}Nd - ^{138}Ce patterns, a trend of global significance. Amongst different models, these distinct patterns can be best explained by the presence of recycled mafic restites from Hadean protocrust in the ancient mantle beneath the Kaapvaal Craton. Further, the data provide unambiguous evidence for the operation of silicate differentiation processes on Earth during the lifetime of ^{182}Hf , i.e., the first 60 million years after solar system formation. The striking isotopic similarity between recycled protocrust and the low ^{182}W endmember of modern OIBs might also constitute the missing link bridging ^{182}W isotope systematics in Archean and young mantle-derived rocks.

Long-term preservation of Hadean protocrust in Earth's mantle

Jonas Tusch¹, J. Elis Hoffmann², Eric Hasenstab¹, Mario Fischer-Gödde¹, Chris S. Marien¹, Carsten Münker¹

¹Institut für Geologie und Mineralogie, Universität zu Köln, Zùlpicher Str. 49b, 50674 Cologne, Germany

²Institut für Geologische Wissenschaften, Freie Universität Berlin, Malteserstraße 74-100, 12249 Berlin, Germany

ABSTRACT

With plate tectonics operating on Earth, the preservation potential for mantle reservoirs from the Hadean Eon (>4.0 Ga) has been regarded as very small. The quest for such early remnants has been spurred by the observation that many Archean rocks exhibit excesses of ^{182}W , the decay product of short-lived ^{182}Hf . However, it remains speculative, if Archean ^{182}W anomalies and also ^{182}W deficits found in many young ocean island basalts (OIBs) mirror primordial Hadean mantle differentiation or just variable contributions from older meteorite building blocks delivered to the growing Earth. Here, we present a high-precision ^{182}W isotope dataset for 3.22-3.55 Ga old rocks from the Kaapvaal Craton, southern Africa. In expanding previous work, our study reveals widespread ^{182}W deficits in different rock units from the Kaapvaal Craton and also the very first discovery of a negative co-variation between short-lived ^{182}W and long-lived ^{176}Hf - ^{143}Nd - ^{138}Ce patterns, a trend of global significance. Amongst different models, these distinct patterns can be best explained by the presence of recycled mafic restites from Hadean protocrust in the ancient mantle beneath the Kaapvaal Craton. Further, the data provide unambiguous evidence for the operation of silicate differentiation processes on Earth during the lifetime of ^{182}Hf , i.e., the first 60 million years after solar system formation. The striking isotopic similarity between recycled protocrust and the low ^{182}W endmember of modern OIBs might also constitute the missing link bridging ^{182}W isotope systematics in Archean and young mantle-derived rocks.

40 Main text

41 Due to plate tectonic processes, the accessible silicate reservoirs on Earth have lost
42 most of their memory of the first ca. 500 Ma of Earth's history. Hence, our
43 understanding of this time period comes from indirect evidence, e.g., from geochemical
44 tracers such as short-lived and now extinct nuclide series that all were only active
45 during the first ca. hundred million years after solar system formation(1–3). The
46 detection of terrestrial variability in the relative abundances of short lived nuclide decay
47 products such as ^{129}Xe , ^{142}Nd , and ^{182}W provided firm evidence that primordial
48 reservoirs were not fully homogenized by mantle-dynamics, and played a significant
49 role during the formation of the first continental crust(3–5). The recent discovery of
50 ^{182}W , ^{142}Nd , and ^{129}Xe anomalies in modern mantle-derived rocks(2, 6, 7)
51 demonstrates that ancient mantle reservoirs are still accessible. Whereas anomalous
52 ^{129}Xe and ^{142}Nd isotope compositions in mantle-derived rocks can primarily be
53 assigned to early planetary outgassing and early silicate differentiation, respectively,
54 the presence of ^{182}W isotope anomalies can result from multiple processes. Negative
55 ^{182}W anomalies in modern ocean island basalts (OIBs), for instance, were interpreted
56 to result from core-mantle interaction(8, 9). In contrast, Archean rocks mainly exhibit
57 elevated ^{182}W compositions. While some interpret prevalent positive ^{182}W anomalies
58 in Archean rocks as a result of disproportional accretion(10), others have pointed out
59 that this view may be an oversimplification as observations from other isotope
60 systematics suggest other processes to be involved. Suggested alternative models
61 invoke metal-silicate segregation or silicate differentiation in an early magma ocean,
62 or during crust-mantle differentiation(11, 12). Others interpreted the elevated ^{182}W
63 isotope compositions as resembling a complementary reservoir to the negative ^{182}W
64 isotope anomalies observed in modern OIBs, arguing that core-mantle interaction has
65 caused a secular change in the average mantle $\mu^{182}\text{W}$ from ca. +13 to 0(9). Although
66 in principle core-mantle interaction may provide a viable explanation for the secular
67 evolution of ^{182}W patterns it remains highly speculative. Hence, other scenarios should
68 also be considered. For instance, isotope anomalies of ^{142}Nd in Archean rocks clearly
69 provide evidence for early silicate differentiation having operated during the Hadean,
70 which may potentially have caused accompanying ^{182}W anomalies(12, 13). However,
71 it has been demonstrated that pristine ^{142}Nd - ^{182}W records are often obscured, either
72 by multistage differentiation processes within the lifetime of ^{146}Sm - ^{142}Nd , after ^{182}Hf -
73 ^{182}W went extinct, or via fluid-controlled second stage metasomatic overprint of
74 primordial ^{182}W patterns(14).

75 To further evaluate the processes that can account for ^{182}W anomalies in Archean
76 rocks, we investigated samples from the eastern Kaapvaal Craton, southern Africa.
77 These lithologies are well suited to search for vestiges of early silicate differentiation,
78 because they were shown to display both heterogeneous ^{142}Nd and ^{182}W
79 compositions(11, 12, 15–17). We performed high-precision ^{182}W isotope analyses on
80 a comprehensive suite of 17 samples that range from mantle-derived lithologies of
81 mafic-ultramafic composition to different types of granitoids. By combining ^{182}W isotope
82 analysis with high-precision isotope dilution measurements for high field strength
83 elements (HFSE), U, and Th, we assessed the sources of the W inventory in mantle-
84 derived rocks. Our samples span an age range from ca. 3.55-3.22 Ga, represent the
85 main lithological units of the Ancient Gneiss Complex (AGC) and also comprise the

oldest rocks of the Barberton Granite-Greenstone terrain (BGGT). Moreover, most of these samples have previously been analyzed for their ^{143}Nd , ^{176}Hf , and ^{142}Nd compositions(15, 18, 19) and some samples were remeasured here as replicates. Following a previous attempt(20) we combined ^{138}La - ^{138}Ce isotope analyses with ^{143}Nd and ^{176}Hf systematics to place further constraints on Hadean mantle differentiation processes. To better understand the depletion history of the Kaapvaal mantle we also investigated ^{143}Nd - ^{176}Hf systematics in ultramafic rocks from the BARB1 and BARB2 drill cores that were dragged during the International Continental Drilling Program (ICDP-2009/01, Exp.ID 5047) in the Komati Formation of the BGGT. These samples were previously shown to exhibit highly variable ^{143}Nd - ^{176}Hf compositions(21). In order to assess if late accreted material affected ^{182}W isotope systematics we also investigated Ru isotope systematics that were recently introduced as a novel tool to decipher the inventory of late accreted material in the source region of mantle rocks(22). More information about the regional geology and samples is provided in SI Appendix.

Measurements of ^{182}W isotope compositions followed previously reported protocols(14, 23) that were slightly modified to yield sufficiently purified solutions for high-precision measurements using a Thermo Fisher Neptune Plus MC-ICP-MS at Cologne. Uncertainties for averages of repeated analysis of sample solutions (95% confidence interval, $n = 6$ -11) range between ± 1.4 ppm and ± 5.1 ppm (average ± 2.7 ppm). Our intermediate precision is inferred from repeated analyses of in-house rock reference materials, also including a 3.27 Ga old komatiite from the Pilbara Craton (sample 160245, Ruth Well Formation), Western Australia, previously shown to display an excess of ^{182}W (23). All in-house rock reference materials were also passed through our separation protocol and measured in every session, yielding $2 \text{ SD} \leq \pm 2.7$ ppm (SI Appendix, Fig. S1). More information about the analytical protocol (including isotope dilution techniques and isotope composition measurements for Hf, Nd, Ce and Ru) is provided in the method section.

Our results for ^{182}W isotope analysis are summarized in SI Appendix Table S1. Major and trace element compositions as well as ^{138}Ce - $^{142,143}\text{Nd}$ - ^{176}Hf and Ru isotope compositions are provided in SI Appendix, Table S2. Irrespective of petrology and provenance (AGC or BGGT), all rock types display ^{182}W isotope compositions that range from modern mantle values ($\mu^{182}\text{W} = 0$) to deficits as low as -9.2 ± 3.2 ppm. While most mantle-derived rocks from the BGGT display $\mu^{182}\text{W}$ values that overlap with the modern mantle value, most mantle-derived rocks from the AGC display resolvable $\mu^{182}\text{W}$ deficits. The distribution and the range of isotope compositions for ^{182}W in our rock samples from the Kaapvaal Craton is similar to that for ^{142}Nd , displaying both, negative and modern isotope composition(15). However, combined ^{182}W - ^{142}Nd data for rocks from the eastern Kaapvaal Craton, also including literature data from the Schapenburg Greenstone Remnant (SGR) adjacent to the BGGT(12), only display a vague co-variation (SI Appendix, Fig. S2), even when only considering samples with pristine W concentrations (i.e., canonical W/Th ratios). Notably, our dataset reveals a negative co-variation of $\mu^{182}\text{W}$ with initial $\varepsilon^{143}\text{Nd}_{(t)}$ and $\varepsilon^{176}\text{Hf}_{(t)}$ for mantle-derived rocks (Fig. 1) which is not observed for $\mu^{142}\text{Nd}$. To our knowledge, this is the first discovery of a co-variation between ^{182}W compositions and long-lived radiogenic nuclides. The observed co-variation for our samples is further strengthened

by literature data for komatiites from the SGR adjacent to the BGGT(12) and the Komati Formation from the BGGT(11, 16). The absence of similar co-variations in other Archean lithostratigraphic successions can either be explained by initial igneous processes that decoupled ^{143}Nd - ^{176}Hf systematics during source overprint(24) or the disturbance of pristine ^{182}W patterns by metasomatic agents during late stage metamorphism(13, 14).

A previous study(14) has shown that pristine ^{182}W isotope signatures can be modified during fluid-mediated second stage enrichment of W. One valuable tool to screen for disturbed elemental W budgets in mantle-derived rocks is the W/Th ratio, which displays a canonical range in pristine magmatic systems (0.09-0.24)(25). The majority of samples analyzed in this study display elevated W/Th ratios reflecting fluid-mediated re-distribution of W during metasomatism, as also evident from negative correlations with Ce/Pb (SI Appendix, Fig. S3). However, although only three mantle-derived rocks studied here reveal undisturbed elemental W systematics ($\text{W/Th} \leq 0.24$), the samples still display ^{182}W co-variations with initial $\epsilon^{143}\text{Nd}_{(t)}$ and $\epsilon^{176}\text{Hf}_{(t)}$ values. These observations indicate that the W redistribution did not significantly change the ^{182}W composition of these samples and was only of localized character, in contrast to previous studies from other Archean Cratons(14, 23). Moreover, co-variations with ^{182}W compositions are also observed for incompatible trace element ratios classically interpreted as immobile, in particular Hf/Sm and Zr/Sm (Figs. 2a+b). In addition, broadly coupled variations with Zr content (SI Appendix, Fig. S4) demonstrate that Hf and REE largely behaved immobile during metamorphism. Consequently, a metasomatic origin of the observed co-variations between ^{182}W and other radiogenic isotopes can be ruled out. As the elements involved display vastly different mobilities at metamorphic conditions, it would be expected that alteration would obscure the observed co-variations rather than forming them.

Most of the samples analyzed in this study also reveal strong correlations between their initial values of long-lived radiogenic isotopes like $\epsilon^{143}\text{Nd}_{(t)}$, $\epsilon^{176}\text{Hf}_{(t)}$ and $\epsilon^{138}\text{Ce}_{(t)}$ (Figs. 3a+b). Only two samples (AGC 38 and ZA-38) display disturbed initial $\epsilon^{138}\text{Ce}_{(t)}$ values but still preserve pristine $\epsilon^{143}\text{Nd}_{(t)}$ and $\epsilon^{176}\text{Hf}_{(t)}$ systematics. Therefore, initial $\epsilon^{138}\text{Ce}_{(t)}$ values for these samples are excluded from further interpretations and are not shown in Fig. 3c. In this regard, combined ^{143}Nd - ^{176}Hf - ^{138}Ce systematics serve as a valuable tool to clarify why two mantle-derived rocks (AGC 350 and ZA-31a, pale red symbols, Fig. 1) slightly deviate from the $\mu^{182}\text{W}$ vs. $\epsilon^{143}\text{Nd}_{(t)}$ and $\epsilon^{176}\text{Hf}_{(t)}$ trends. The deviation of these samples towards more negative ^{182}W compositions most likely reflects that in some rare cases metasomatic agents redistributed W between different reservoirs. As the observed co-variations of $\mu^{182}\text{W}$ with $\epsilon^{143}\text{Nd}_{(t)}$ and $\epsilon^{176}\text{Hf}_{(t)}$ are defined by mafic-ultramafic volcanic rocks, it is obvious that the observed trend reflects mixing between different mantle-source reservoirs. One mantle endmember exhibits no resolvable ^{182}W isotope anomalies at near chondritic initial $\epsilon^{143}\text{Nd}_{(t)}$ and $\epsilon^{176}\text{Hf}_{(t)}$ values, most likely representing near primitive mantle. The other endmember is best characterized by komatiites from the SGR that exhibit the largest ^{182}W isotope deficits extending to -11.4 ppm and strongly elevated initial $\epsilon^{143}\text{Nd}_{(t)}$ and $\epsilon^{176}\text{Hf}_{(t)}$ values of up to +2.6 and +6.2, respectively(12). It is surprising that felsic samples from the Kaapvaal Craton plot on the same trend as mafic samples, suggesting short residence times between emplacement of the mafic protolith and formation of felsic orthogneisses

(open symbols SI Appendix, Fig. S5).

Our high-precision Ru isotope measurements for two komatiites from the Dwalile Greenstone Remnant (AGC 83 & AGC 86) reveal that the Archean mantle in the Kaapvaal Craton already has a modern mantle-like Ru isotope composition and does not show coupled ^{100}Ru - ^{102}Ru excesses that were recently reported for 3.8-3.7 Ga old Archean rocks from SW Greenland. The distinct Ru isotope signature inferred for the SW Greenland rocks was interpreted to reflect a mantle source that did not receive the full complement of late accreted material(22). In contrast, the modern mantle-like Ru isotope composition of the Dwalile komatiites indicates that the Kaapvaal mantle source by 3.46 Ga had already completely equilibrated with the full complement of late accreted material (SI Appendix, Figs. S6 & S7).

In the following discussion, we will largely focus on the origin of the low ^{182}W endmember. As we will show, the low ^{182}W endmember may provide novel insights into the secular evolution of the ^{182}W isotope composition of Earth's mantle. In particular, we evaluate, if present-day mantle plumes with their characteristic ^{182}W deficit may be modern analogues of the low ^{182}W endmember from the Kaapvaal Craton. So far, the presence of ^{182}W deficits has been explained as the consequence of several processes. These include (i) equilibration of the mantle source with anomalously large amounts of late accreted material (late accretion hypothesis), (ii) by core-mantle interaction(8, 9, 26), or (iii) early fractionation of Hf from W by silicate crystal-liquid fractionation, e.g., in an early magma ocean(11).

The late accretion hypothesis has been postulated to explain the relative and absolute abundances of highly siderophile elements (HSE) in the bulk silicate Earth (BSE) by the addition of about 0.5% of chondritic material after core formation(27, 28). Late accretion would not only have affected the HSE budget of the BSE but also its ^{182}W isotope composition(3). Accordingly, some portions of the Archean mantle could have remained in disequilibrium(29), and mantle domains that did not fully equilibrate with late accretionary components, would be characterized by positive ^{182}W isotope anomalies and HSE abundances that are lower than the modern BSE. Consequently, negative ^{182}W isotope anomalies would imply excesses of late accreted components that should also be reflected in unusually high HSE contents. However, absolute HSE abundances in the mantle source of the SGR-like endmember with its large ^{182}W deficit, were only estimated to amount to ca. 30% of those in the present-day BSE(12, 30). The depleted mantle source of the SGR komatiites may provide an explanation here, where the PGE depletion may indicate sulfur undersaturated melting conditions(30). At such conditions, mainly iridium-like platinum-group elements (IPGE: Os, Ir, Ru), that are hosted by refractory platinum group minerals (PGM), remain to large degrees in the source(31). This leaves an open possibility for the ^{182}W isotope deficits reflecting an excess of late accreted components. However, our constraints from Ru isotopes clearly demonstrate that the ambient mantle in the Kaapvaal Craton did not receive unusual amounts of late accreted components (SI Appendix, Fig. S7). Moreover, a mantle source that experienced full sulfur exhaustion would likely be extremely depleted in W, making a direct contribution to the ^{182}W inventory of the Kaapvaal rocks unlikely.

An alternative explanation for negative ^{182}W isotope anomalies in Archean rocks like those from the Kaapvaal Craton may be offered by recent studies on OIBs. It has been

proposed that prevalent negative ^{182}W isotope anomalies in modern, plume-derived OIBs result from chemical and isotopic equilibration between their mantle sources and the outer core without affecting HSE abundances(8, 9, 26). For the same reasoning outlined above, we regard such a scenario as unlikely. A mantle source that experienced full sulfur exhaustion by large degrees of melt extraction would likely be extremely depleted in W, an incompatible lithophile element, making a direct contribution to the ^{182}W inventory of the Kaapvaal rocks unlikely. Moreover, the modern mantle-like Ru isotope signatures in our samples is not in support of an isotopic equilibration between mantle and core material. Based on previous constraints on the Ru isotope composition of the pre-late veneer mantle(22), the Ru in the core would most likely be characterized by a ^{100}Ru excess. Notably, selective addition of W via core-mantle interaction is not the only explanation for the negative ^{182}W anomalies in modern OIBs. Noble gas work on modern mantle-derived rocks rather suggested that the source reservoirs must have had differentiated from the convecting mantle very early prior to 4.45 Ga(5, 32, 33). The concurrent ^{182}W isotope anomalies in the modern mantle may therefore also reflect in-situ decay of ^{182}Hf (i.e., during the first ca. 60 Ma after solar system formation). The presence of such ancient mantle reservoirs and the role of mantle plumes in the past, in particular their contribution to the secular evolution of the ^{182}W isotope composition in the BSE has so far only poorly been constrained. Notably, it has been argued that Archean mafic-ultramafic sequences like those in the BGGT also originate from a mantle plume setting(34). In this regard, mantle-derived rocks from the Kaapvaal Craton may have preserved vestiges of ancient mantle heterogeneities, similar to young OIBs.

It has been postulated that recycling of crustal material is responsible for the geochemical and isotopic variability in modern plume related OIBs(35). In the case of the Kaapvaal Craton, however, direct recycling of ancient protocrust formed during the first ca. 60 Ma appears unlikely, because in this case the negative ^{182}W and ^{142}Nd anomalies should be coupled with unradiogenic ^{143}Nd and ^{176}Hf compositions. In this regard, the coupled depletions of ^{182}W and ^{142}Nd and Hf-Nd isotope patterns led previous studies(12, 17) to conclude that the komatiites from the SGR derived from a mantle domain that was enriched very early (ca. 30 Ma after solar system formation) in highly incompatible elements as a result of fractionating a Mg- and Ca-perovskite mineral assemblage in an early magma ocean. When originally proposed(12) this conclusion was mainly based on apparently decoupled initial $\epsilon^{143}\text{Nd}_{(t)}$ and $\epsilon^{176}\text{Hf}_{(t)}$ compositions of BGGT rocks(16, 21) that were particularly observed in rocks from the Komati Formation (see black symbols in SI Appendix Fig. S11). However, more recent work re-investigated mafic-ultramafic samples from the BGGT (Komati, Sandspruit, Theespruit Formations)(18) and AGC (Dwalile Greenstone Remnant)(19) by employing more sophisticated sample dissolution protocols, yielding considerably less scatter (see red symbols in SI Appendix Fig. S11). By extending this more recent work we re-investigated initial $\epsilon^{143}\text{Nd}_{(t)}$ and $\epsilon^{176}\text{Hf}_{(t)}$ compositions in ultramafic rocks from the BARB1 and BARB 2 cores that were drilled into the Komati Formation and previously reported to exhibit strongly decoupled ^{143}Nd - ^{176}Hf systematics(21). In fact, together with komatiites from the SGR(12), the new data now fall on a trend closely resembling the modern mantle array(36), in line with the consideration that the terrestrial Hf-Nd mantle array has already been established on the early Earth(37) (Fig. 3a and Fig. S11). In line with our results for ^{143}Nd - ^{176}Hf , initial $\epsilon^{138}\text{Ce}$ and $\epsilon^{143}\text{Nd}$ systematics also

271 closely fall on the modern terrestrial array(38). On the basis of available literature data,
 272 we cannot rule out that other mafic units in the BGGT (e.g. Weltevreden, see blue field
 273 in SI Appendix Fig. S11) do indeed preserve an extreme decoupling in their $\epsilon^{143}\text{Nd}$ and
 274 $\epsilon^{176}\text{Hf}$ systematics and anomalous $\epsilon^{138}\text{Ce}$. However, a recent study on the 3.33 Ga
 275 Commondale komatiites from the Kaapvaal Craton demonstrates that decoupled
 276 ^{143}Nd - ^{176}Hf patterns are not unique to magma ocean relics but can also be generated
 277 via hybrid melting of depleted mantle and garnet-pyroxenites in the stability field of
 278 garnet(20, 39). On the basis of more rigorous modelling, employing updated sets of
 279 partition coefficients(40, 41) and by adopting a previous model for SGR komatiites(12),
 280 we therefore re-evaluated the control of perovskite segregation and subsequent mantle
 281 depletion on the ^{143}Nd - ^{176}Hf - ^{138}Ce - and ^{142}Nd isotope inventory (details are provided in
 282 the method section and calculations in Table S3). Herein, a primitive mantle undergoes
 283 removal of 10% perovskite cumulate (Ca:Mg-perovskite 5:95) at 4.537 Ga before it
 284 evolves until 4.027 Ga. Subsequently, this reservoir undergoes melt depletion at 4.027
 285 Ga before it melts at 3.55 Ga to produce the SGR komatiites. In Fig. 3, we show the
 286 evolution of such mantle source compositions recalculated to 3.55 Ga in ^{143}Nd - ^{176}Hf
 287 (Fig. 3b) and ^{143}Nd - ^{138}Ce space (Fig. 3d) as a function of variable Ca:Mg-perovskite
 288 proportions (Ca:Mg-perovskite from 20:80 to 0:100). Considering that melt depletion at
 289 4.027 Ga took place in the garnet stability field, the modelled results for ^{143}Nd - ^{176}Hf
 290 (Fig. 3) are in reasonable agreement with the SGR komatiites. However, fractionating
 291 a Ca:Mg-perovskite assemblage of 5:95 as previously suggested(12) does not lead to
 292 suprachondritic Lu/Hf and to a decoupling of initial $\epsilon^{143}\text{Nd}$ and $\epsilon^{176}\text{Hf}$ systematics, once
 293 recalculated to 3.55 Ga. Rather, the Hf-Nd composition of the modeled mantle after
 294 perovskite segregation is near chondritic at 3.55 Ga. It is the second stage
 295 differentiation step in the garnet stability field at 4.027 Ga that generates the $\epsilon^{143}\text{Nd}$ -
 296 $\epsilon^{176}\text{Hf}$ systematics observed in SGR komatiites. This finding and the fact that mantle-
 297 derived rocks from the Kaapvaal Craton follow the modern-day terrestrial Hf-Nd array
 298 suggests that this array has already started to form in the Archean, as a consequence
 299 of deep mantle melting and an increased role of residual garnet as well as early crustal
 300 recycling(37, 42). The negligible impact of fractionating 10% perovskite cumulate on
 301 magma compositions becomes even more obvious when the incompatible trace
 302 element budgets of both reservoirs are plotted relative to primitive mantle (SI Appendix,
 303 Fig. S8). More important, the relative proportions of Ca- and Mg-perovskite in the
 304 cumulate exert a strong influence on ^{143}Nd - ^{176}Hf systematics(24). It becomes apparent
 305 that ^{176}Hf - ^{143}Nd decoupling strongly depends on the proportion of Ca-perovskite
 306 crystallizing with Mg-perovskite. However, co-precipitation of Ca- and Mg-perovskite
 307 during 10% fractional crystallization remains an open issue and this is highly unlikely
 308 as Ca-perovskite does not appear as first liquidus phase at lower mantle
 309 conditions(43–45). Collectively, we conclude that ^{143}Nd - ^{176}Hf isotope systematics in
 310 the Kaapvaal rocks are non-diagnostic for fractionation of perovskite cumulates. Most
 311 importantly, the perovskite model has difficulties to explain why ^{142}Nd compositions in
 312 mantle-derived rocks from the Kaapvaal Craton do not correlate with ^{143}Nd - ^{176}Hf
 313 compositions.

314 Based on the considerations above, a two-stage process is clearly required where the
 315 negative ^{182}W and ^{142}Nd anomalies formed early and the radiogenic ^{143}Nd and ^{176}Hf
 316 compositions were established after the short-lived systems went extinct. Our
 317 preferred geodynamic model is illustrated in Fig. 4, a detailed description is given in

the method section and all model parameters and calculations are provided in Table S3. Our model is inspired by previous studies on the formation mechanisms of early continental crust(46–48). Accordingly, after formation of a mafic protocrust (Fig. 4a) intra-crustal fractionation lead to the formation of a felsic, TTG-like crust and mafic lower crustal restites that are recycled into the mantle due to their high densities. Here they mechanically and chemically interact with mantle peridotites, producing hybrid mantle reservoirs (Fig. 4b). These hybrid reservoirs may either be probed by deep rooted mantle plumes from lower mantle regions(49) or assimilated in the upper mantle during plume upwelling(50) (Fig. 4c). Melting of such hybrid reservoirs in conjunction with near primitive mantle may account for the compositional trend between long-lived decay systems and ^{182}W , as observed for mafic rocks from the Kaapvaal Craton. In this scenario, the near primitive mantle endmember is characterized by the Barberton komatiites and the hybrid mantle endmember is characterized by the SGR komatiites. As demonstrated below, such mixing relationships provide a viable explanation for the negative co-variation between short- and long-lived radiogenic systems. Moreover, our model can also explain the incompatible trace element systematics in our samples and the SGR komatiites (SI Appendix, Figs. S4 and S12).

Following constraints from phase equilibrium and trace element modeling, melting of Archean TTG suites from mafic protocrust leaves behind residual assemblages of amphibolitic, garnet-amphibolitic or garnet-pyroxenitic composition(51). Figure 4a illustrates that during stage 1 mafic protocrust that formed 50 Ma after solar system formation developed strongly unradiogenic isotope compositions, in particular for the short-lived decay products ^{182}W and ^{142}Nd . Subsequent TTG melting (stage 2 in Fig 4a) leaves behind garnet-rich restites(52), and depending on the timing of this second event, the residual restites will develop towards markedly different ^{142}Nd isotope compositions with time. In contrast, the ^{182}W isotope composition will be insensitive to the timing of TTG extraction, because ^{182}Hf went extinct shortly after formation of the protocrust. Evidence for the presence of such ancient TTG precursors in the Kaapvaal Craton comes from Hf-in-zircon isotope data(53–55) and from rare Hadean detrital zircons in the ca. 3.3 Ga Fig Tree Formation(56) that suggest formation of a felsic protocrust already by the Eoarchean or late Hadean. Moreover, a recent study investigated ^{182}W isotope systematics in diamictites from the Kaapvaal Craton and revealed that the exposed upper continental crust at that time must have had negative ^{182}W compositions(57). Due to the longer half-lives of their parent nuclides, ^{143}Nd and ^{176}Hf isotope compositions in the restites integrate a larger time span and develop much less heterogeneity with time than ^{142}Nd , which can only be formed over a smaller time interval until ^{146}Sm becomes extinct. These considerations explain, why ^{142}Nd signatures became quite variable, depending on the time of TTG extraction, unlike long-lived Hf-Nd compositions that persistently developed towards slightly radiogenic values over time.

It becomes apparent from Fig. 5a that lower crustal restites from ancient protocrust can explain why the ^{143}Nd and ^{176}Hf isotope compositions are so tightly correlated with ^{182}W but not with ^{142}Nd . Recycling of such restites into the mantle formed a hybrid source that is best approximated by compositions of Schapenburg komatiites, which formed through high-degree melting. We found that 10-20% of restites admixed to depleted mantle already reproduce the radiogenic isotope compositions found in the SGR

endmember (Fig. 5b). Once this hybrid mantle source is mixed with primitive material supplied by ascending mantle plumes, it can account for the systematic coupling between initial $\epsilon^{143}\text{Nd}_{(t)}$ - $\epsilon^{176}\text{Hf}_{(t)}$ and $\epsilon^{143}\text{Nd}_{(t)}$ - $\epsilon^{138}\text{Ce}_{(t)}$ (Fig. 3) and also for the opposing variations of ^{182}W (Fig. 1). Exact modeling of ^{138}La - ^{138}Ce systematics is hampered by their poorly constrained behavior during mantle melting, where La-Ce behave highly incompatible and modelled La/Ce is extremely dependent on melt porosity. Notably, our proposed model can well reproduce the incompatible trace element compositions and reconcile distinct trace element features that are diagnostic for the SGR komatiites. As shown in SI Appendix Fig. S12 our modeling results are in good agreement with the SGR komatiites originating from 20-30% batch melting of a hybrid source that consists of depleted mantle and 10-20% lower crustal restites. Moreover, our model can reproduce distinct Hf/Sm and Zr/Sm values prominent within SGR komatiites and their co-variation with ^{182}W isotope compositions (Figs. 2a+b). A recent study on mantle-derived rocks from the Kaapvaal Craton(17) reported a similar correlation of Hf/Sm with ^{142}Nd compositions arguing that this feature is unique to deep magma ocean crystallization processes that happened soon after Earth accretion. Our lower crustal restite model can now offer an alternative explanation. The hybrid source model can also explain the positive initial $\gamma^{187}\text{Os}$ of the SGR komatiites ($\gamma^{187}\text{Os} = +3.7 \pm 0.3(30)$). As discussed in the method section, Re-Os systematics in our modelled reservoirs are more difficult to constrain, resulting in large propagated uncertainties for modelled ^{187}Os compositions. However, our first principle assumptions reveal that the addition of ca. 10-13% restite from Hadean protocrust to a depleted mantle source is in accord with previous models explaining positive initial $\gamma^{187}\text{Os}$ values in modern plume-related basalts and Archean komatiites by the presence of recycled eclogitic or pyroxenitic components in their mantle sources(49, 58). As for ^{187}Os , modelling Pb isotopes, which are often used to assess crustal recycling in mantle sources, involves many uncertainties (e.g. hydrothermal redistribution) that irretrievably lead to large propagated errors in modelling approaches. Therefore, we conclude that Pb isotopes are not a diagnostic tool to identify Hadean crustal restites (see also method section).

In conclusion, the isotope patterns found here for Kaapvaal Craton rocks are clearly unique within the Archean rock record, and they may be locally restricted. However, the lower crustal restite model for the Kaapvaal Craton presented in this study has global implications as it provides an intriguing explanation of ^{182}W isotope variations in modern OIBs and provides additional constraints on the secular evolution of ^{182}W isotope systematics in mantle-derived rocks through deep time. A recent study(59) has proposed that the global ^{182}W dataset for OIBs can be explained by the admixture of the classical mantle endmember components DMM (depleted MORB mantle), EM1 (enriched mantle I), EM2 (enriched mantle II), and HIMU (high “ μ ” or $^{238}\text{U}/^{204}\text{Pb}$) to a primordial reservoir that is characterized by negative ^{182}W anomalies and depleted $^{143}\text{Nd}/^{144}\text{Nd}$ composition. Remarkably, lower crustal restites, formed between 4.35 and 4.25 Ga from ancient mafic protocrust constitute a viable endmember for the global OIB array in $\mu^{182}\text{W}$ - $^{143}\text{Nd}/^{144}\text{Nd}$ space (Fig. 6), once calculated to present day $^{143}\text{Nd}/^{144}\text{Nd}$. We therefore speculate, that lower crustal restites from Hadean protocrust were delaminated and ultimately recycled into the mantle. Following recent models, such crustal remnants might have accumulated at the lower-upper mantle boundary and picked up by rising mantle plumes(50). Alternatively they could have passed the lower-upper mantle boundary descending into the lower mantle where they might have

become part of large low shear-wave velocity provinces (LLSVPs) in the present day mantle that are interpreted to contribute to rising mantle plumes(60). Indeed, it has been shown that the modeled restite has the potential to delaminate into the mantle due to its density contrast compared to ambient mantle(52). Recent thermomechanical and thermodynamic modelling showed that garnet-rich assemblages will descend through the lower-upper mantle boundary and sink into the lower mantle(61). Accordingly, geophysical studies demonstrated that LLSVPs may represent mixtures of recycled dense material that accumulated at the core-mantle boundary(62, 63). Taking into consideration that the strongly depleted restites would exhibit low He abundances, recycling of this component into the lower mantle would not significantly affect the $^3\text{He}/^4\text{He}$ ratios of a primordial undegassed host-reservoir. Correspondingly, the observed coupled variations between $^3\text{He}/^4\text{He}$ ratios and $\mu^{182}\text{W}$ (6, 8) would simply reflect variable proportions of such a hybrid lower mantle reservoir in ascending mantle plumes that partially melt at high degrees at upper mantle conditions. In this regard, our model provides an alternative explanation for the origin of negative ^{182}W isotope anomalies in modern OIBs and bridges ^{182}W isotope systematics in Archean mantle-derived rocks with observations from modern-day mantle plumes. Our discovery of long-term preservation of Hadean protocrust in Earth's mantle has also other far-reaching implications, in that their presence requires silicate reservoirs on Earth to have already differentiated during the lifetime of ^{182}Hf (11).

Materials and Methods

Lower Hadean protocrust delamination model

The starting compositions, applied partition coefficients, respective mineral assemblages, references for decay constants and reservoir compositions, and calculations are listed in SI Appendix, Table S3. In our model we always used internally consistent sets of partition coefficients and assumed batch melting throughout(64). Isotope compositions for ^{138}Ce , ^{143}Nd and ^{176}Hf were modeled by using parent-daughter ratios from the calculated sources, the appropriate decay constants(65–68) and assuming CHUR composition for the BSE(69, 70). The isotope compositions for ^{142}Nd and ^{182}W were back calculated by using the appropriate decay constants(71, 72), present-day isotope composition for the BSE(73, 74), elemental Hf/W and Sm/Nd ratios for the BSE(25, 75), and solar-system initials for the parent-daughter ratios(76, 77). Formation of a mafic protocrust is stage 1 of our model (Fig 3a). The maximum age for the extraction of our protocrust is set by core formation, which could have been completed as early as 38 Ma after solar system formation(25). We assume extraction of mafic protocrust 50 Ma after solar system formation from a mantle with BSE composition(75). The timing of protocrust formation particularly affects the isotope compositions of the short-lived isotope systems during further protocrust evolution (Fig. 5a). For protocrust formation, we used a consistent set of experimental partition coefficients for REE, HFSE, and Th assuming 20% batch melting at 2 GPa(41). Partition coefficients for W are often incomplete in the literature. If not available, we calculated partition coefficients for W by using partition coefficients for mineral phases from experiments on garnet lherzolite(78) that were adjusted to the melt conditions in

our model by using appropriate partition coefficients for Th. Both elements were shown to behave similarly incompatible during silicate crystal-liquid fractionation(25). Correspondingly, the W/Th ratio of our modeled melts extracted from the primitive mantle ($W/Th = 0.14$) is indistinguishable from the canonical range reported in the literature(25).

At 4.35-4.25 Ga, (stage 2) we re-melt our modeled mafic protocrust (Fig. 4b) and calculate (based on an experimental study(52)) the composition of a typical garnet-rich restite that remained after lower crustal anatexis of a metamorphosed basaltic assemblage (estimated to be representative for the Hadean protocrust) at 12 kbar, in equilibrium with ca. 21% tonalitic melt. The timing of TTG formation as well as the residual mineral assemblage exerts a strong influence on the ^{142}Nd evolution. In contrast, the ^{182}W isotope composition will not change because the ^{182}Hf - ^{182}W system went functionally extinct shortly after protocrust formation at ca. 60 Ma after solar system formation. Due to the enriched composition of the precursor and the long half lives of their parent isotopes, prolonged tonalite formation will only cause small variations in isotopic ingrowth for ^{143}Nd and ^{176}Hf in the lower crustal restites (Fig. 5a). Therefore, prolonged tonalite formation can explain decoupling of ^{142}Nd from the other isotope systems in the residual garnet-rich restites and provides an explanation why ^{143}Nd and ^{176}Hf correlate so tightly with ^{182}W but not ^{142}Nd . Indeed, the occurrence of rare Hadean detrital zircons(56) and Hf isotope data in zircon reported for Paleoarchean grey gneisses of the eastern Kaapvaal Craton reveal incorporation of older continental crustal rocks with Eoarchean to late Hadean age(53–55) that have not been directly preserved in the rock record of the Kaapvaal Craton. In addition, detrital platinum group minerals (PGM) sampled from sedimentary units of the Kaapvaal Craton reveal Re-depletion ages up to 4.1 Ga(79), hinting on remnants of Hadean protocrust within the Kaapvaal Craton. Moreover, diamictites from the Kaapvaal Craton were found to preserve a negative ^{182}W signature(57), hinting at a upper continental crust with negative ^{182}W composition. Assuming prolonged tonalite formation initiated by ca. 4.35 Ga and continued for 100 Myrs the variation of ^{142}Nd isotope composition within their restites would be ca. 9 μ units at 3.55 Ga. In contrast, ^{143}Nd and ^{176}Hf would not vary by more than 1 ϵ unit.

Previous studies found evidence for incorporation of recycled mafic crustal material into melts derived from hybrid mantle plumes throughout Earth's history(49, 58, 80, 81). Moreover, it has previously been shown that delamination of crustal restites into depleted mantle can cause melting of hybrid mantle sources and that the resulting trace element signatures resemble those of typical komatiites(47). Likewise, we propose here the mechanical incorporation of 10-20 % of garnet-rich restites into an ascending plume that taps depleted mantle sources at ca. 3.55 Ga. Twenty to thirty percent of batch melting of such a hybrid source can reproduce the trace element compositions of the SGR komatiites (SI Appendix, Fig. S12). We attribute the variation within the SGR komatiite suite and their partially more depleted trace element compositions, compared to the modeled patterns, to olivine accumulation as indicated by co-variations between MgO content and incompatible trace element concentrations (not shown). For the upwelling mantle plume into which the restites were mixed we assume 10% melt depletion at ca. 3.85 Ga. We use coherent, experimentally constrained melting parameters(41) to calculate the isotope and trace element composition at 3.55 Ga, the age of our samples. The modeled depleted mantle displays

initial $\epsilon^{143}\text{Nd}$ and $\epsilon^{176}\text{Hf}$ values of +4.3 and +7.9, respectively, which is in perfect agreement with the modern terrestrial Hf-Nd array(36), within the range of the modeled DMM composition at 3.55 Ga(82) and also consistent with observational constraints from mantle-derived rocks from the Kaapvaal Craton(39). The isotope compositions for ^{182}W , ^{142}Nd , ^{143}Nd , and ^{176}Hf of 20-30% melts extracted from a hybrid plume source, containing 10-20% of restite and corresponding proportions of plume derived melt, is in accord with the range of isotope compositions observed in SGR komatiites (see Fig. 5b and SI Appendix, Table S3). It is noteworthy that the ^{182}W isotope composition of the melt is controlled by the restite because high modal abundances of garnet and amphibole, together with refractory Ti-rich phases (rutile/ilmenite), result in high bulk partition coefficients for W. This buffers the ^{182}W isotope composition against possible variations in the ambient Archean mantle (on average ca. +13 ppm(14, 23)). Variable proportions of rutile or ilmenite as a residual Ti-rich phase in the restites do not significantly affect the results of our model. Ratios of Nb/Ta have been proven to be valuable indicators to discriminate between rutile and ilmenite(83), but unfortunately, no Ta concentrations are available for SGR komatiites. We expect ilmenite being present in the restites as this results in reasonable Nb/Th ratios (Nb/Th = 14.8-15.1) that are similar to the range observed in the SGR komatiites (Nb/Th = 11.2-14.6). Evidence for the presence of lower crustal restites in the mantle source of the SGR komatiites is also provided by Zr/Sm (and Hf/Sm) ratios that are best explained by fractionation of garnet. The co-variation of Zr/Sm (and Hf/Sm) with ^{182}W isotope composition is perfectly reproduced by our model (Fig. 2b).

The hybrid plume model can also explain the ^{187}Re - ^{187}Os isotope inventory of the SGR komatiites. The komatiite lavas from Schapenburg exhibit overall low PGE abundances and sample a melt depleted, sulfur exhausted mantle source(30), which is supported by correlations between the IPGE (Os, Ir, Ru) with lithophile elements such as La (not shown). However, the positive initial $\gamma^{187}\text{Os}$ of the SGR komatiites ($\gamma^{187}\text{Os} = +3.7 \pm 0.3$) require that their mantle source evolved with a time-integrated suprachondritic Re/Os(30). A conceptual model for ^{187}Os isotope systematics is presented in Table S3 applying the same time evolution path as for the other decay systems (Fig. 5). In brief, we modelled the ^{187}Os isotope composition of a melt that derived from a depleted mantle source and assimilated delaminated restite which remained behind after TTG melt extraction of a Hadean protocrust. The Re and Os abundances and $^{187}\text{Re}/^{187}\text{Os}$ of the Hadean protocrust are difficult to estimate because Re and Os can be highly variable within metamorphosed mafic crust ranging from ca. 2-1700 pg/g Re and 0.9-12 pg/g Os, yielding $^{187}\text{Re}/^{187}\text{Os}$ from ca. 5 to 2700(84). To circumvent this uncertainty, we used average Re-Os compositions of typical flood basalt samples from the Otong Java Plateau (Kwaimbaita Formation) that derived from a primitive mantle source by magmatic differentiation, yielding ca. 1.2 ppb Re and 0.06 ppb Os and an average $^{187}\text{Re}/^{188}\text{Os}$ of 90(80). Using these Re-Os abundances, the Hadean protocrust had developed a highly radiogenic $\gamma^{187}\text{Os}$ between ca. 2800 and 4400 until partial melting between 4.35-4.25 Ga (TTG melt formation). We assume that most of the Re in the protocrust was extracted during TTG formation through complete sulfide consumption(85). However, trace amounts of Re may be held back in residual garnet, where Re is compatible(86, 87). Considering previous melt depletion for the plume-related mantle reservoir, the Re budget of the modelled hybrid reservoir can be assumed to be fully controlled by the restite. We therefore use the average Re

concentration in the SGR komatiites (36 ppt(12, 30)) as minimum estimate for the Re concentration of the restite. Further, we assume that Os within the restite was fully retained by accessory chromite and magnetite(88). Correspondingly, after TTG formation, the restite retained a radiogenic $\gamma^{187}\text{Os}$ (3.55) between ca. 2950 and 4450, when applying a $^{187}\text{Re}/^{188}\text{Os}$ of 2.7.

Our constraints from Ru isotopes show that the PGE inventory in the SGR komatiites does not reflect a mantle source that lacks significant amounts of late accreted components. More likely, the overall low PGE abundances reflect residual platinum group minerals (PGM) in a melt-depleted source that lead to very low $^{187}\text{Re}/^{187}\text{Os}$ ratios (≤ 0.005) assuming low Re concentrations (ca. 0.001 ng/g) and depleted mantle-like Os compositions (0.8-9 ng/g(89)). Considering that melt depletion occurred at 3.85 Ga, this mantle source would develop to a $\gamma^{187}\text{Os}$ of ca. -21 at 3.55 Ga. As previously proposed the SGR komatiite lavas contain ca. 1.1 ng/g Os(30). This comparably low concentration can be explained, if PGM or refractory alloys remained in the sulfur exhausted source(30) holding back a large amount of Os-Ir-Ru. Our model calculations show that the assimilation of ca. 10-13% restite to the komatiite melt can reproduce the radiogenic $\gamma^{187}\text{Os}$ values observed in the SGR komatiite suite (SI Appendix, Table S3 and Fig. S9).

Similar to the other decay systems, the involvement of a TTG formation event during the Hadean is necessary to explain the $\gamma^{187}\text{Os}$ values of the Schapenburg komatiites at 3.55 Ga (Table S3). Without such an event, the protocrust would have developed to extreme $\gamma^{187}\text{Os}$ values of ca. 15000, which would dominate the SGR komatiites. These conceptual assumptions are also in accord with other plume-derived magmatic systems where radiogenic Os isotope compositions have been interpreted as being derived from hybrid plumes that incorporated a pyroxenite or eclogite component(49, 58, 80).

As an additional system to assess incorporation of Hadean restites in the komatiite melt, we also modelled the Pb isotope composition. However, it is difficult to evaluate if these Hadean restites that were recycled into the mantle carry a diagnostic Pb isotope composition. From mineral partition coefficients alone, it is expected that restites complementary to TTGs would exhibit strongly anomalous Pb isotope compositions. By a “first-order” estimate (for calculations see Table S3) we assume a single-stage Pb evolution starting at 4.567 Ga with a μ ($^{238}\text{U}/^{204}\text{Pb}$) of 8.5 and a α_0 ($^{206}\text{Pb}/^{204}\text{Pb}_{\text{initial}}$) of 9.307(90). Restites that remained after partial melting of a mafic protocrust (TTG formation at 4.35 Ga) would develop towards an unradiogenic $^{206}\text{Pb}/^{204}\text{Pb}$ composition due to a low $\mu^{238}\text{U}/^{204}\text{Pb}$ of ~ 3.7 and display a present-day $^{206}\text{Pb}/^{204}\text{Pb}$ of only ~ 14.3 . The complementary TTGs would exhibit an elevated $\mu^{238}\text{U}/^{204}\text{Pb}$ of ~ 10.2 and evolve towards radiogenic present-day $^{206}\text{Pb}/^{204}\text{Pb}$ compositions (~ 22.1). However, Pb isotope systematics during partial melting of hydrated oceanic crust are not only entirely controlled by mineral partition coefficients as the elements involved (U, Th and Pb) display different redox sensitivities and reveal a different mobility in the presence of fluids(91). It is therefore very likely that U-Pb isotope systematics were often affected by ocean floor processes resulting in highly variable initial Pb isotope compositions in Archean TTGs and their mafic counterparts. Indeed, while many Archean cratons have preserved a long-lived high- μ continental

lithosphere with distinctive Pb-isotope compositions(92), other cratons show large Pb isotope variations with more unradiogenic Pb isotope patterns(93–95).

Assessment of magma ocean models involving perovskite fractionation

Alternative models have been proposed for the origin of the SGR komatiites(12), involving fractionation of a high-pressure and temperature Mg- and Ca-perovskite mineral assemblage in an early terrestrial magma ocean. In short, we found that such models are highly dependent on the sets of partition coefficients used and the choice of Ca:Mg-perovskite assemblages. Independent of this issue, some important diagnostic features of the samples analyzed here (e.g., ^{142}Nd - ^{176}Hf - ^{143}Nd isotope relationships) cannot be reproduced by a magma ocean model or do not require the presence of perovskite cumulates at all.

In detail, we modeled evolution of a mantle reservoir that has undergone perovskite segregation, tightly following a previous model for the SGR(12). Herein, a primitive mantle undergoes removal of 10% perovskite (5:95% Ca:Mg-perovskite) at 4.537 Ga before it evolves until 4.027 Ga. Subsequently, this reservoir undergoes batch melting in the spinel stability field at 4.027 Ga before it melts at 3.55 Ga to produce the SGR komatiites. For perovskite, we used a more rigorous, internally consistent set of partition coefficients from reference 40 using laser ICPMS data for their representative experiment H2020 a+b and relative abundances of Mg and Ca perovskite of reference 12. Mantle depletion at 4.027 Ga was modeled in analogy to the parameters presented by reference 12, but again using more updated sets of partition coefficients(41). All other parameters like decay constants or CHUR values are as above. We refrained from modeling W because the original dataset for perovskite(40) does not include W partition coefficients. Previous modeling(12) referred to lattice strain modeling of D_W , but the lattice strain model used by reference 40 is only applicable to 1+, 2+, 3+, and 4+ ions. Recent work(96, 97) has shown that the valence state of W, even in the more reduced regime of an early magma ocean, is rather 6+.

Hafnium-Nd-Ce modeling results are shown as blue symbols in Fig. 3, recalculated to 3.55 Ga. It is important to note, that the fractionation of perovskite during magma ocean crystallization does not lead to suprachondritic Lu/Hf and to a decoupling of $\epsilon^{143}\text{Nd}$ and $\epsilon^{176}\text{Hf}$ systematics, once recalculated to 3.55 Ga. Rather, the Hf-Nd composition of the modeled mantle after perovskite segregation is near chondritic at 3.55 Ga. Depletion of such a mantle reservoir at 4.027 Ga in the spinel stability field yields decoupled Hf-Nd isotope compositions, but at extremely radiogenic $\epsilon^{143}\text{Nd}$ at a given $\epsilon^{176}\text{Hf}$ (SI Appendix, Table S3), which is nowhere found in our sample set. Larger amounts of residual garnet during mantle depletion at 4.027 Ga may result in $\epsilon^{143}\text{Nd}$ - $\epsilon^{176}\text{Hf}$ systematics that resemble the compositions of SGR komatiites, in analogy to the modern-day terrestrial mantle array(36). Rather, this finding is in line with the consideration that the origin of the terrestrial Hf-Nd mantle array has already been established in the early Earth as a consequence of deeper mantle melting and an increased role of residual garnet or recycling of garnet-bearing restites(37). Moreover, the choice of Ca-Mg perovskite assemblages exerts a strong influence on the decoupling of ^{143}Nd and ^{176}Hf isotope systematics(24). To better illustrate these effects, we show the evolution of modelled SGR komatiite source compositions in ^{143}Nd - ^{176}Hf

and ^{143}Nd - ^{138}Ce space in response to variable Ca-Mg perovskite assemblages (Ca:Mg-perovskite from 20:80 to 0:100). It becomes apparent that the decoupling of ^{176}Hf from ^{143}Nd strongly depends on the amount of Ca-perovskite crystallizing together with Mg-perovskite. However, the co-precipitation of Ca- and Mg-perovskite during an initial 10% of fractional crystallization remains an open issue as Ca-perovskite does not appear as first liquidus phase at lower mantle conditions(43, 44). Most importantly, the model cannot explain why ^{142}Nd compositions in mantle-derived rocks from the Kaapvaal Craton do not correlate with ^{143}Nd - ^{176}Hf compositions.

A popular way to verify if perovskite fractionation took place is to inspect trace element ratios that behave sensitive to perovskite fractionation. However, as Ca perovskite fractionates many trace elements in the opposite way as Mg-perovskite(40), many of the geochemical signatures often referred to are actually non-diagnostic. For example, Hf/Sm in rocks from the Kaapvaal Craton were taken as evidence supporting the hypothesis that ^{142}Nd anomalies result from fractionating perovskite in a deep magma ocean(17). However, when considering different proportions of Ca-Mg perovskite and taking into consideration that the absolute amount of fractionated perovskite may vary it is possible to generate a large range of Hf/Sm ratios (SI Appendix, Fig. S10a). This clearly demonstrates that trace element ratios should be used that are largely insensitive to the choice of Ca-Mg perovskite proportions (e.g. Zr/Nb). However, models that only fractionate a small fraction of perovskite(12) do even not fractionate such element ratios, thus withstanding such investigations (SI Appendix, Fig. S10b).

Collectively, our modeling of a mantle reservoir involving perovskite segregation and subsequent mantle depletion demonstrate that ^{143}Nd - ^{176}Hf isotope systematics are non-diagnostic features to identify perovskite fractionation and cannot explain the full range of isotope compositions found in our sample set and previously published isotope data for the SGR komatiite suite.

Analytical protocol

Our analytical protocol for isotope dilution analysis follows procedures that were described in detail by previous studies(23, 98, 99). For ^{138}La - ^{138}Ce measurements we processed 1g of sample powder. For La-Ce isotope dilution (ID) measurements a 5% aliquot was spiked with a ^{138}La - ^{142}Ce isotope tracer. For the 95% aliquot we utilized the first stage cation resin column of a previously published protocol for W(14) to separate REE from matrix elements for high-precision ^{138}Ce isotope composition (IC) measurements. This step is required since sample loads larger than 200mg exceed the capacity of the first stage column in our ^{138}La - ^{138}Ce separation protocol(99). Measurement protocols for La-Ce ID measurements as well as for Ce IC measurements followed a previously described routine(99) except that $10^{12} \Omega$ resistors used for interference corrections were replaced by $10^{13} \Omega$ resistors. All data were normalized relative to $^{136}\text{Ce}/^{140}\text{Ce}$ of 0.002124072(100) and are given relative to a $^{138}\text{Ce}/^{136}\text{Ce}$ value of 1.33738 for the Mainz AMES standard solution(101). All samples were analyzed repeatedly. Reported uncertainties either refer to the corresponding 95% CI ($n \geq 4$) or to our intermediate precision ($\pm 0.21 \epsilon$ -units)(20).

Details about the chemical separation and purification protocol of Ru are described elsewhere(22) and involved NiS fire assay digestion, cation column chemistry and

microdistillation. High-precision Ru isotope composition measurements were conducted on a Thermo Fisher Neptune Plus MC-ICP-MS at University of Cologne following a previous protocol(22). In short, ~ 100 ng/ml solutions were introduced at an uptake rate of ca. 50 μ l/min using a PFA nebulizer and a Cetac Aridus II desolvating system. Measurements comprised 100 integrations of 8.4 s and were preceded by an on-peak baseline (40 integrations of 4.2 s) on a solution blank (0.28 M HNO₃). The data were internally corrected for mass bias by using $^{99}\text{Ru}/^{101}\text{Ru} = 0.7450754$ and utilizing the exponential law. Sample solutions were always bracketed by measurements of a concentration-matched Ru standard solution (Alfa Aesar Ru) to report relative Ru isotope compositions in the μ -notation, which gives the part per million deviation for $^i\text{Ru}/^{101}\text{Ru}$ isotope ratios between a sample and bracketing standard solutions. The accuracy of the Ru isotope measurements was evaluated by the repeated analysis of replicate digestions of a 2.05 Ga chromitite from Bushveld igneous complex (UG-2) and two 3.8 Ga chromitites from the Itsaq gneiss complex, SW Greenland (194856, 194857), that were previously shown to display modern-mantle like and anomalous Ru isotope compositions, respectively(22). Our Ru isotope data obtained for all three chromitites agree well with previously reported data(22) (SI Appendix Fig. S6). The uncertainty for measurements is either given as the external uncertainty of the method(22) (2 s.d. for samples measured $n < 4$ times) or the corresponding 95% confidence interval (if $n \geq 4$).

High-precision ^{182}W isotope measurements mainly followed established analytical protocols(14, 23) that were slightly modified to yield highly purified W solutions from large sample loads (up to 18g) and to improve our analytical uncertainty. In short, samples were measured at average signal intensities of 17 V for ^{182}W (using 10^{11} Ohm amplifiers) corresponding to a ~175 ng/ml W sample solution at an uptake rate of ca. 55 μ l/min. Samples were always bracketed by a concentration-matched certified reference material (NIST SRM 3163). Results of high-precision W isotope analyses are reported in the μ -notation (equivalent to ppm) relative to the bracketing NIST solutions and always refer to the measured $^{182}\text{W}/^{184}\text{W}$ ratio that has been corrected for mass bias by using $^{186}\text{W}/^{184}\text{W} = 0.92767(102)$. All samples were repeatedly analyzed ($n=6-11$) and uncertainties for average W isotope compositions are correspondingly reported as 95% confidence intervals (see SI Appendix, Table S1). Our protocol for the chemical purification of W for high-precision isotope composition analysis comprises four columns. During a cation (AG 50 W-X8 resin, column I) and anion exchange stage (AG 1-X8 resin, column II) W is separated from matrix elements and HFSE & Ti, respectively. Columns III (TEVA resin) and IV (TODGA resin) are clean up columns that yield purified W cuts. In this regard, the repetition of the final stage column during the chemical separation of W(23) improves the purification from remaining matrix elements. The final W-bearing eluate was directly loaded onto BioRad Poly-Prep® columns filled with 0.8ml Eichrom prefilter® material to extract organic compounds. This, together with threefold treatments with 80 μ l of cHNO_3 -30% H_2O_2 at max. 60°C after dry-down steps during and after the chemical separation, strongly improved yields and removed mass independent effects on ^{183}W (14). Prior to loading onto our final stage column, we combined up to 10 cuts in case sample powders were split up into aliquots (up to 1.3g) during matrix separation. The combination of sample solutions during chemical separation does not affect the accuracy of our high-precision ^{182}W isotope analysis as demonstrated by

indistinguishable results for sample solutions of our in-house rock reference material LP 1 (historical La Palma Basalt), that were either obtained from single column cuts (up to 1.3g) or combined solutions from 10 column cuts (in total 11.3 g). The purpose of combining the final cuts is to efficiently measure the cuts by reducing the cumulative volume of leftovers after multiple measurements of individual solutions. This allows measuring at the highest beam intensities possible and, together with our refined separation procedure, significantly improves the analytical uncertainty of our measurements. This is also reflected by our intermediate precision of our in-house rock reference materials LP 1 and AGC 351 that were always measured in every session, yielding markedly improved 2 SD of ± 1.5 ppm and ± 2.7 ppm, respectively (SI Appendix, Fig. S1). The $\mu^{182}\text{W}$ session averages for LP 1 (1480 OIB from La Palma) and AGC 351 (3455 Ma gneiss from Swaziland) overlap within their 95% CI (LP1 = -0.4 ± 1.0 ppm and AGC 351 = -0.2 ± 0.5 ppm) and are indistinguishable from the NIST reference material and previously reported long-term averages for the same sample powders(14, 23). Additionally, we also performed repeated analyses ($n = 15$) of a 3.27 Ga old Komatiite (sample 160245, Ruth Well Formation) from the Pilbara Craton Western Australia that exhibits highly elevated W concentrations of $19.1 \mu\text{g/g}$ (23). The $\mu^{182}\text{W}$ session average for sample 160245 ($\mu^{182}\text{W} = +7.9 \pm 0.7$ ppm, 95% CI) is in agreement with previous results(23) and shows a good intermediate precision (2 SD of ± 2.5 ppm). This, together with the elevated ^{182}W isotope composition and high W concentration of sample 160245 validates the method for analytical campaigns addressing ^{182}W isotope systematics in Archean mantle-derived rocks that often display anomalous ^{182}W isotope compositions.

Competing interest statement

The authors declare no competing interest.

Acknowledgments

J.T. and C.M. acknowledge funding through the European Commission by ERC grant 669666 ‘Infant Earth’. MFG and JT acknowledge funding by DFG grant FI 1704/5-1. JEH acknowledges funding by DFG grant HO4794/1-2. We thank Frank Wombacher for maintenance of the MC-ICP-MS and for managing the clean-lab. We are grateful to Mike Jansen for helpful discussions. We thank Allan Wilson for contributing ICDP (2009/01, Exp.ID 5047) samples from the Komati Formation.

Figures

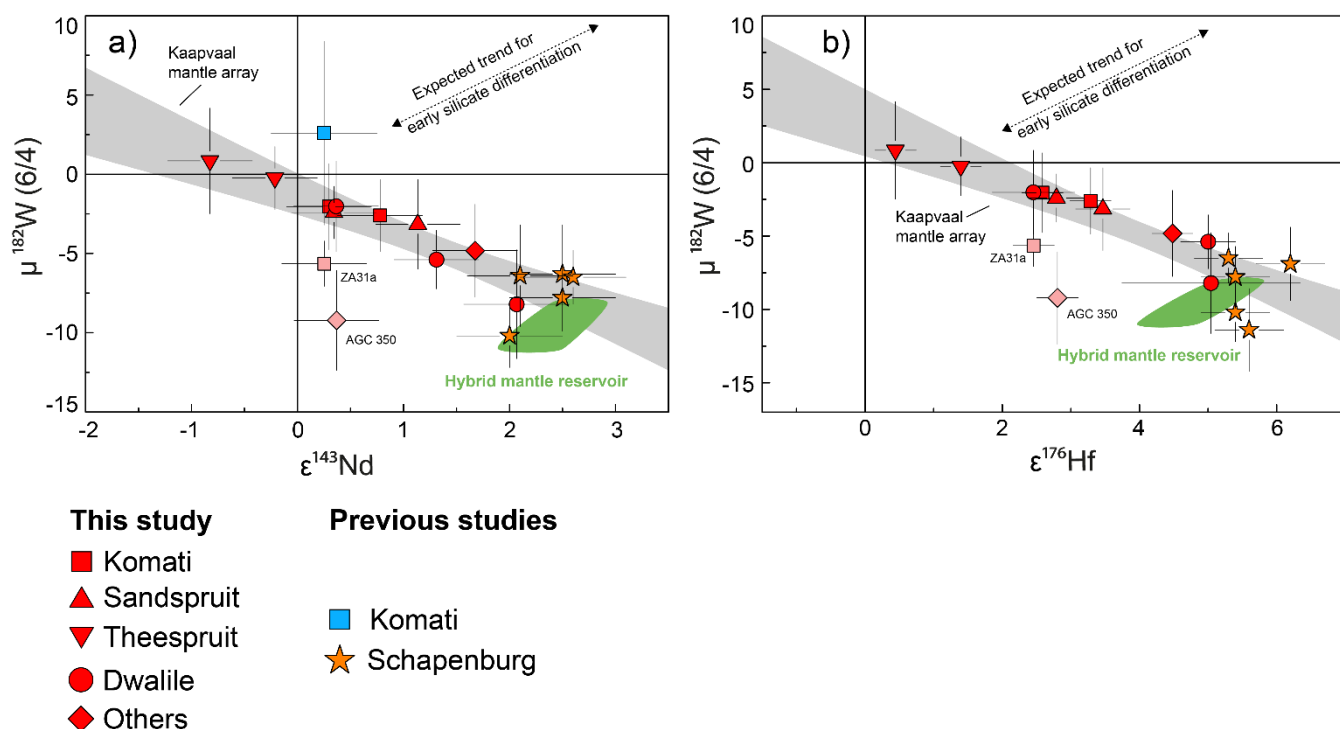


Fig. 1: Measured $\mu^{182}\text{W}$ vs. $\epsilon^{143}\text{Nd}_{(t)}$ (a) and $\mu^{182}\text{W}$ vs. $\epsilon^{176}\text{Hf}_{(t)}$ (b) for mantle-derived mafic rock samples from the Kaapvaal Craton including literature data. The ^{182}W isotope composition for sample AGC 350 and ZA31a (pale red symbols) were most likely overprinted by metasomatic agents carrying negative ^{182}W isotope compositions. The literature data include previously published data for komatiites from the Schapenburg Greenstone Remnant (orange asterisks)(12) and the Komati Formation (blue square)(11, 16). We note that previously published literature data for the Komati Formation only report combined $\mu^{182}\text{W}$ vs. $\epsilon^{143}\text{Nd}_{(t)}$ data for one single sample (sample BV 02, blue square)(11, 16). The green fields illustrate modeled values of our proposed hybrid reservoir (10-20% restites admixed to depleted mantle). The shaded grey field, referred to as *Kaapvaal mantle array*, is an uncertainty envelope employing the 95% confidence interval in which of all mantle-derived samples are expected to fall. Note, that the negative co-variation displayed by the *Kaapvaal mantle array* does not follow the expected trend for early silicate differentiation (indicated by dashed line in panel 1b).

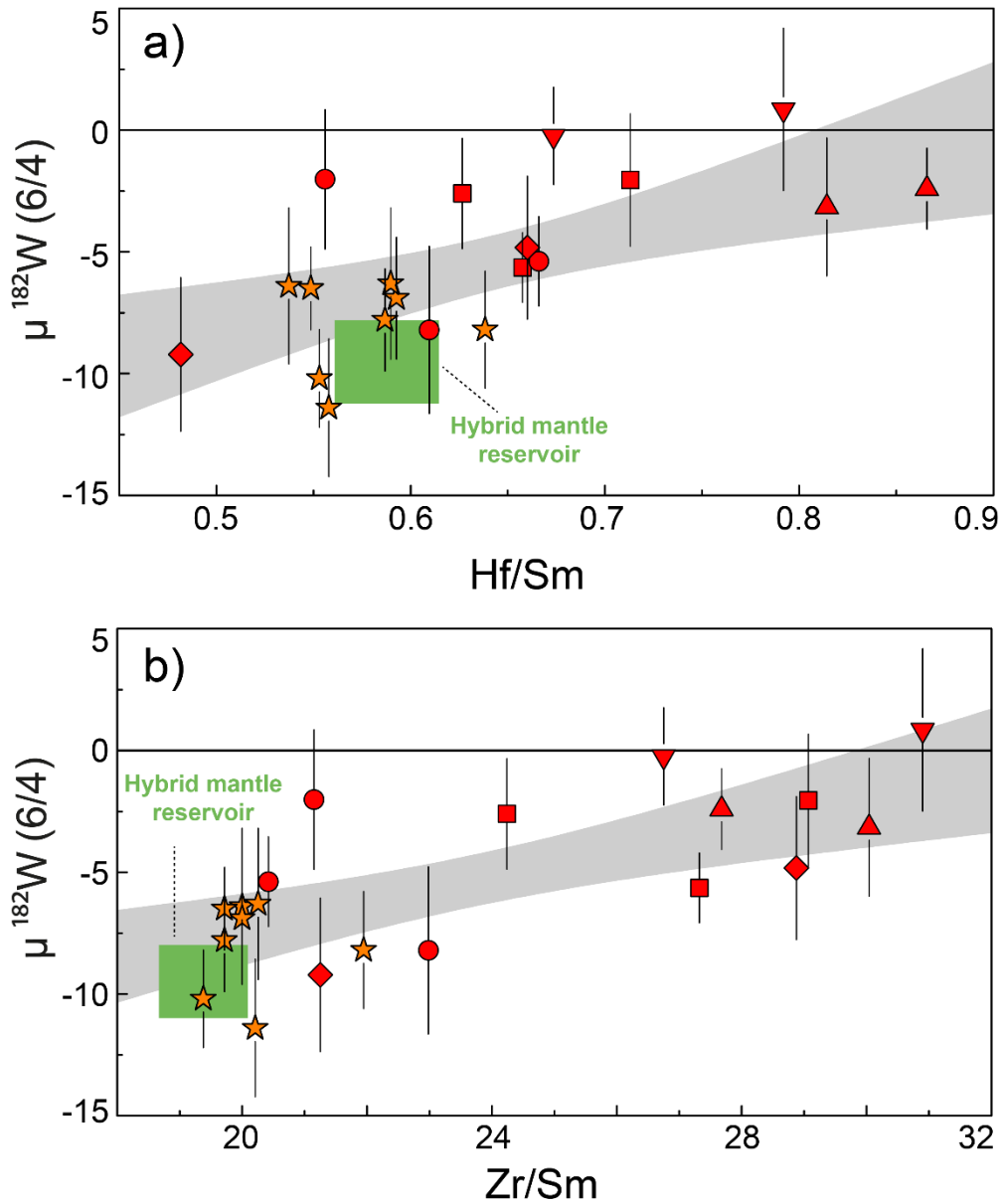


Fig. 2: Plot of $\mu^{182}\text{W}$ vs. (a) Hf/Sm and (b) Zr/Sm for rocks from the Kaapvaal craton. Symbols are the same as in Fig. 1. Data for komatiites from the Schapenburg Greenstone Remnant (SGR) were taken from the literature(12). The combined data indicate a systematic co-variation between ^{182}W isotope composition and Hf/Sm, Zr/Sm ratios with one endmember defined by the SGR komatiites. The negative $\mu^{182}\text{W}$ anomalies and low Hf/Sm and low Zr/Sm ratios prominent in the SGR komatiites can be attributed to the presence of 10 – 20% garnet-rich restites within a hybrid source that underwent 20 – 30% batch melting (green box). The grey shaded array refers to the 95% confidence interval in which all samples are expected to fall.

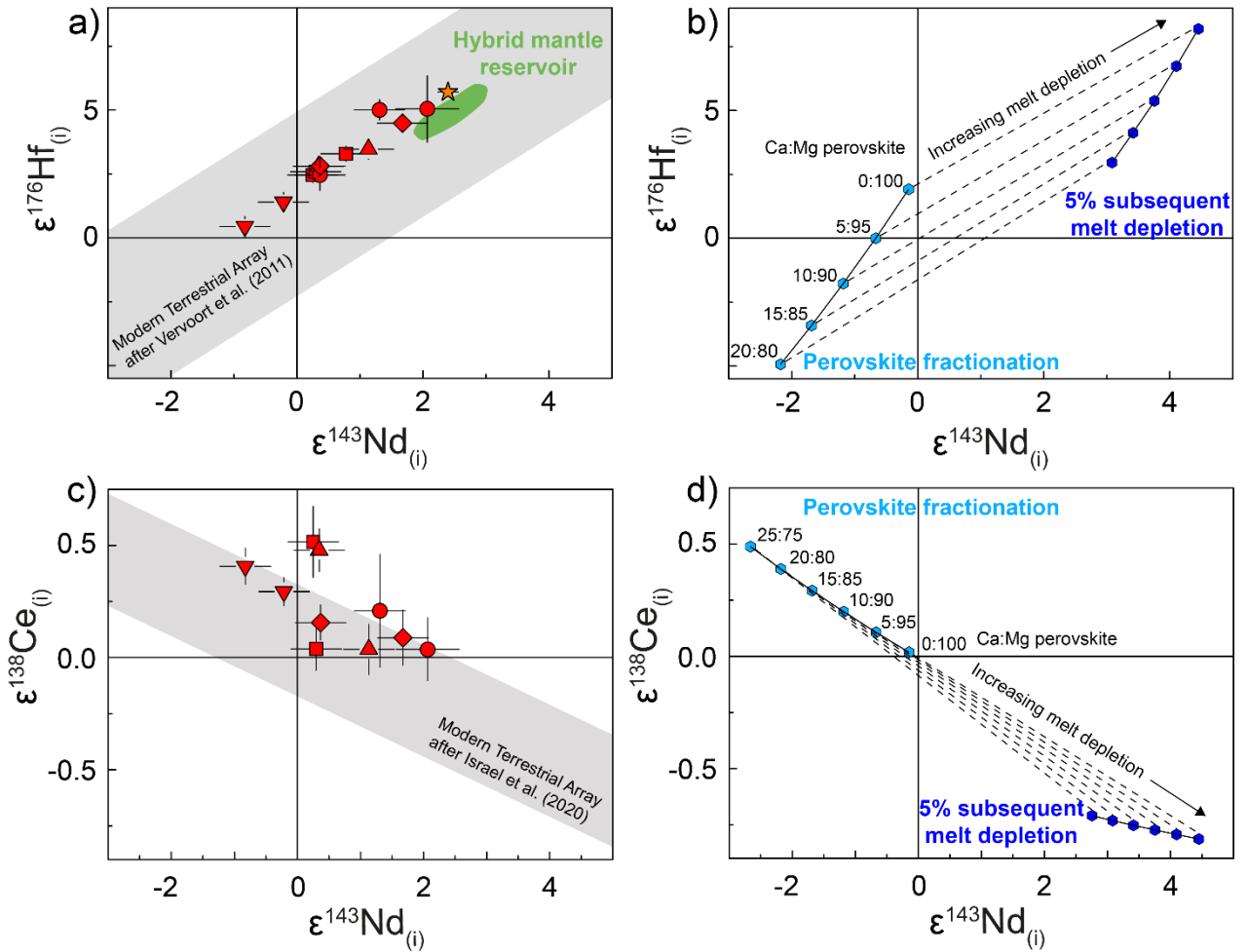


Fig. 3: Plot of $\epsilon^{176}\text{Hf}_{(t)}$ vs. $\epsilon^{143}\text{Nd}_{(t)}$ (a+b) and $\epsilon^{143}\text{Nd}_{(t)}$ vs. $\epsilon^{138}\text{Ce}_{(t)}$ (c+d) for mantle-derived mafic-ultramafic rocks from the Kaapvaal Craton analyzed in this study (red symbols in panels a+c) and for modelled compositions involving perovskite fractionation (blue symbols in panels b+d). Symbols are the same as in Fig. 1. The green fields illustrate modelled values of our proposed hybrid mantle reservoir (10-20% restites admixed to depleted mantle). Blue symbols illustrate our modelling results for mantle reservoirs (at 3.55 Ga) that underwent perovskite segregation (pale blue symbols) and subsequent melt depletion (using an internally consistent set of partition coefficient, see method section) in the garnet stability field (dark blue symbols) illustrating that ^{143}Nd - ^{176}Hf systematics are no diagnostic features to identify perovskite fractionation in an early magma ocean. The grey bands in panels a and c show the modern Terrestrial Array for MORBs and OIBs ($\epsilon\text{Hf} = 1.55 \times \epsilon\text{Nd} + 1.21$ and $\epsilon\text{Ce} = -0.14 \times \epsilon\text{Nd} + 0.05$) (36, 38). The $\epsilon^{138}\text{Ce}_{(t)}$ of the modeled hybrid reservoir is not shown in (c) due to large modeling uncertainties imparted by the highly incompatible behavior of La and Ce.

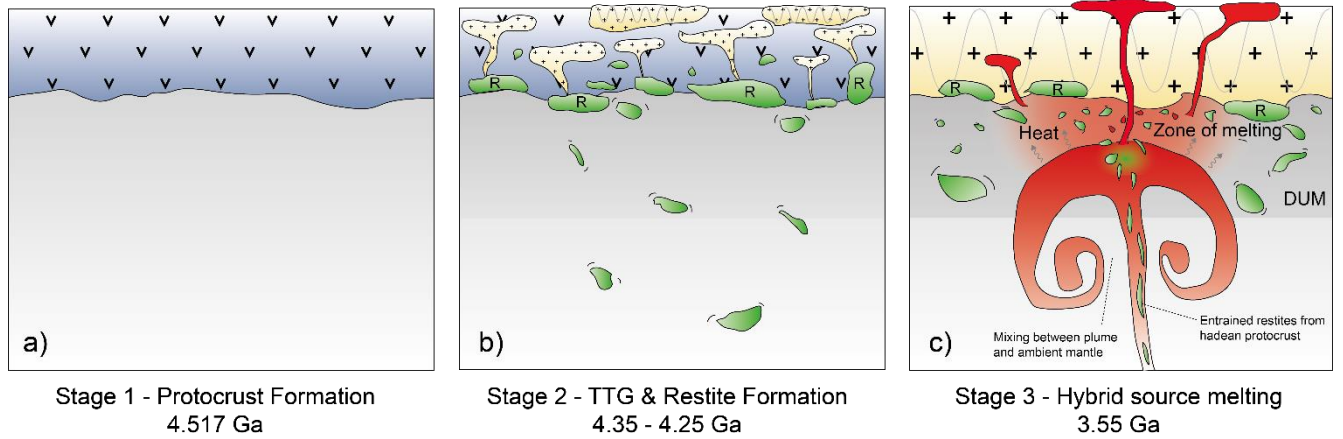


Fig. 4: Preferred geodynamic model for the origin of crustal and mantle-derived rocks from the Kaapvaal Craton. (a) Formation of a mafic protocrust by ca. 50 Ma after solar system formation. (b) Formation of TTG-like batholiths (orange) and residual garnet-rich restites (green, labelled „R“) after partial protocrustal anatexis between ca. 4.35 and 4.25 Ga. (c) Recycling of lower crustal restites and plume initiated volcanism lead to melting of hybrid sources that involved delaminated restites, depleted and primitive mantle supplied by the ascending plume. Shades of grey visualize depleted upper mantle (DUM) and lower mantle (light grey). Note that delaminated restites may either be probed by deep rooted mantle plumes from lower mantle regions or be assimilated in the upper mantle by ascending plumes.

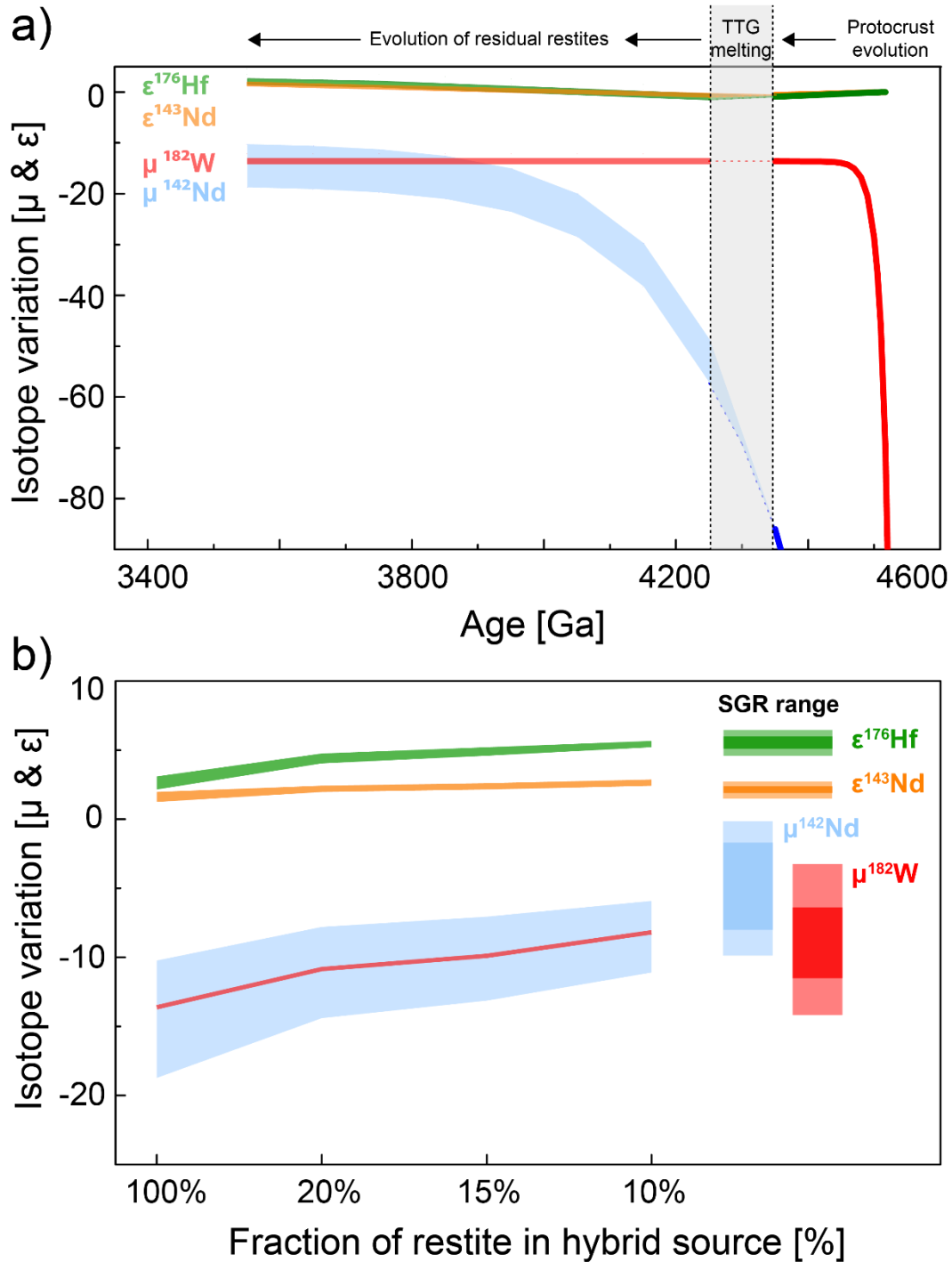


Fig. 5: Isotope evolution graphs for the proposed geodynamic model involving mantle recycling of lower crustal restites. (a) During stage 1, mafic protocrust formed ca. 50 Ma after solar system formation developed strongly unradiogenic isotope compositions, in particular for ^{182}W and ^{142}Nd . Stage 2 marks restite formation during TTG extraction from mafic protocrust. The grey bar illustrates the time interval (4.35 to 4.25 Ga) over which TTG extraction affects the isotope compositions of residual restites. Depending on the exact timing of TTG extraction, the restites develop to markedly different ^{142}Nd isotope composition with time (blue field). In contrast, ^{182}W is insensitive to the timing of TTG extraction, because ^{182}Hf went extinct shortly after formation of the mafic protocrust. Due to their longer half lives the effects on long-lived radionuclides are rather negligible. (b) Mixing calculations illustrating the isotope composition of the proposed hybrid reservoirs as a function of delaminated restites mixed into depleted mantle. Ca. 10-20% of admixed restite to depleted mantle reproduces the isotope compositions found in the SGR endmember. This hybrid source mixed with primitive mantle material supplied by ascending mantle plumes as reflected in the *Kaapvaal mantle array* for ^{182}W and long-lived radiogenic nuclides (see Fig. 1).

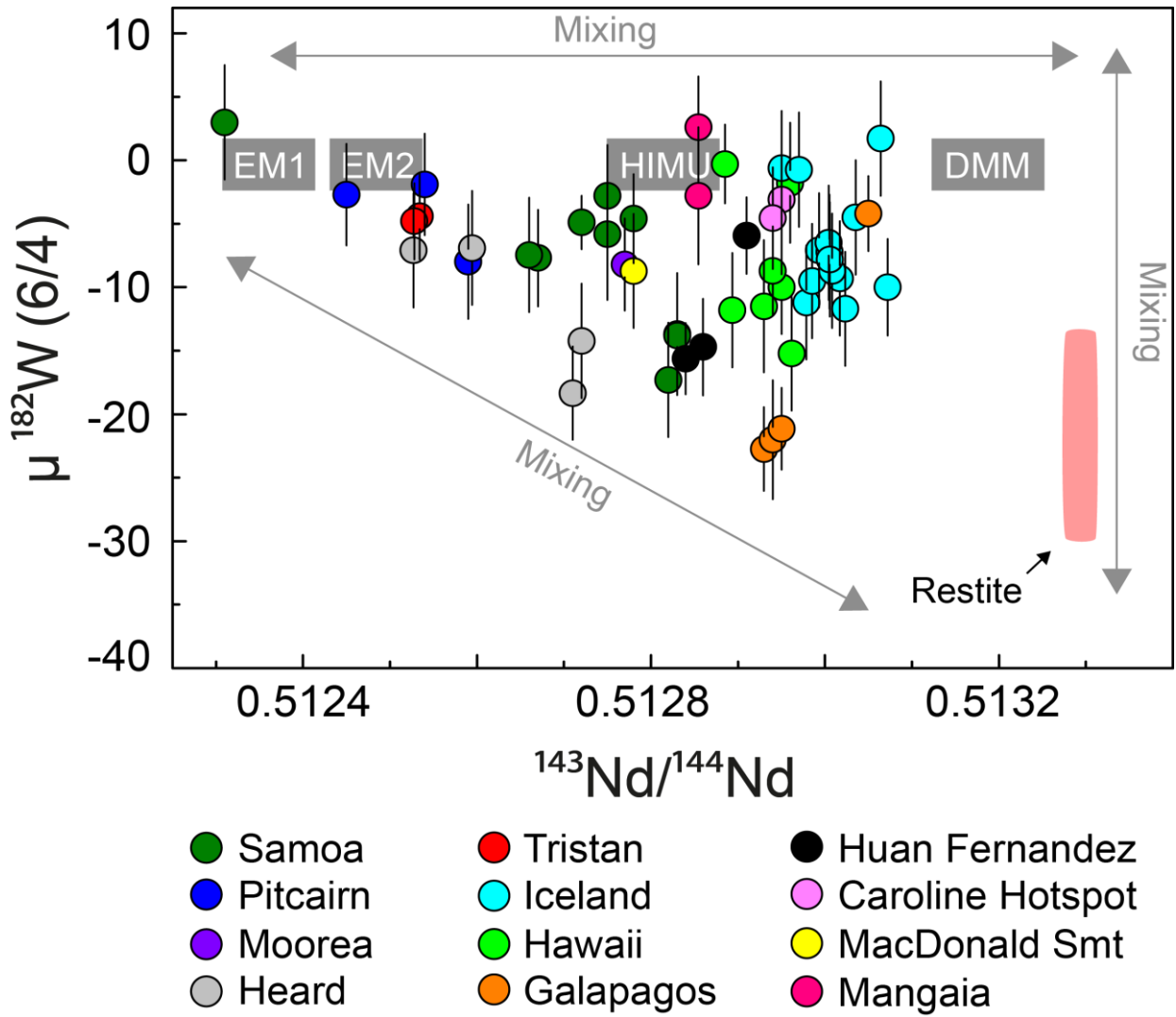


Fig. 6: Compilation of combined ^{182}W and ^{143}Nd isotope data available for modern OIBs. Data were compiled from recent studies(8, 59) and references therein. Notably, the global compilation for modern OIBs shows a similar pattern than the Archean mantle-derived rock assemblage from the Kaapvaal Craton including an endmember with low $\mu^{182}\text{W}$ and radiogenic $^{143}\text{Nd}/^{144}\text{Nd}$. Also shown is the present ^{182}W and ^{143}Nd isotope composition calculated for Hadean restites that remained isolated in the mantle (pink field). This global dataset can be best explained by the admixture of the classical mantle endmember components DMM (depleted MORB mantle), EM1 (enriched mantle I), EM2 (enriched mantle II) and HIMU (high “ μ ” or high $^{238}\text{U}/^{204}\text{Pb}$) to a primordial reservoir that is characterized by negative ^{182}W anomalies and depleted ^{143}Nd isotope composition. A similar OIB compilation for ^{182}W and ^{176}Hf is limited by the availability of ^{176}Hf isotope data but shown for comparison in SI Appendix, Fig. S14.

References main text

1. C. L. J. Harper, S. B. Jacobsen, Evidence from coupled ^{147}Sm - ^{143}Nd and ^{146}Sm - ^{142}Nd systematics for very early (4.5-Gyr) differentiation of the Earth's mantle. *Nature* **360**, 728–732 (1992).
2. S. Mukhopadhyay, Early differentiation and volatile accretion recorded in deep-mantle neon and xenon. *Nature* **486**, 101–4 (2012).
3. M. Willbold, T. Elliott, S. Moorbath, The tungsten isotopic composition of the Earth's mantle before the terminal bombardment. *Nature* **477**, 195–198 (2011).
4. G. Caro, B. Bourdon, J. Birck, ^{146}Sm – ^{142}Nd evidence from Isua metamorphosed sediments for early differentiation of the Earth ' s mantle. *Nature* **423**, 428–431 (2003).
5. C. Allègre, T. Staudacher, P. Sarda, Rare gas systematics: formation of the atmosphere, evolution and structure of the Earth's mantle. *Earth Planet. Sci. Lett.* **81**, 127–150 (1987).
6. A. Mundl, *et al.*, Tungsten-182 heterogeneity in modern ocean island basalts. *Nature* **69**, 66–69 (2017).
7. B. J. Peters, R. W. Carlson, J. M. D. Day, M. F. Horan, Hadean silicate differentiation preserved by anomalous $^{142}\text{Nd}/^{144}\text{Nd}$ ratios in the Réunion hotspot source. *Nature* **555**, 89–93 (2018).
8. A. Mundl-Petermeier, *et al.*, Anomalous ^{182}W in high $^3\text{He}/^4\text{He}$ ocean island basalts: Fingerprints of Earth's core? *Geochim. Cosmochim. Acta* **271**, 194–211 (2020).
9. H. Rizo, *et al.*, ^{182}W evidence for core-mantle interaction in the source of mantle plumes. *Geochemical Perspect. Lett.* **11**, 6–11 (2019).
10. G. J. Archer, *et al.*, Lack of late-accreted material as the origin of ^{182}W excesses in the Archean mantle : Evidence from the Pilbara Craton , Western Australia. *Earth Planet. Sci. Lett.* **528**, 115841 (2019).
11. M. Touboul, I. S. Puchtel, R. J. Walker, ^{182}W Evidence for Long-Term Preservation of Early Mantle Differentiation Products. *Science (80-.)*. **335**, 1065–1070 (2012).
12. Puchtel, J. Blichert-Toft, M. Touboul, M. F. Horan, R. J. Walker, The coupled ^{182}W - ^{142}Nd record of early terrestrial mantle differentiation. *Geochemistry Geophys. Geosystems* **17**, 2168–2193 (2016).
13. Rizo, *et al.*, Early Earth Differentiation Investigated Through ^{142}Nd , ^{182}W , and Highly Siderophile Element Abundances in Samples From Isua, Greenland. *Geochim. Cosmochim. Acta* **175**, 319–336 (2016).
14. J. Tusch, *et al.*, Uniform ^{182}W isotope compositions in Eoarchean rocks from the Isua region, SW Greenland: the role of early silicate differentiation and missing late veneer. *Geochim. Cosmochim. Acta* **257**, 284–310 (2019).
15. K. P. Schneider, J. E. Hoffmann, M. Boyet, C. Münker, A. Kröner, Coexistence of enriched and modern-like ^{142}Nd signatures in Archean igneous rocks of the

- 1001 eastern Kaapvaal Craton, southern Africa. *Earth Planet. Sci. Lett.* **487**, 54–66
1002 (2018).
- 1003 16. I. S. Puchtel, *et al.*, Insights into early Earth from Barberton komatiites:
1004 Evidence from lithophile isotope and trace element systematics. *Geochim.*
1005 *Cosmochim. Acta* **108**, 63–90 (2013).
- 1006 17. M. Boyet, M. Garçon, N. Arndt, R. W. Carlson, Z. Konc, Residual liquid from
1007 deep magma ocean crystallization in the source of komatiites from the ICDP
1008 drill core in the Barberton Greenstone Belt. *Geochim. Cosmochim. Acta* **304**,
1009 141–159 (2021).
- 1010 18. K. P. Schneider, *et al.*, Petrogenetic evolution of metabasalts and
1011 metakomatiites of the lower Onverwacht Group, Barberton Greenstone Belt (
1012 South Africa). *Chem. Geol.* **511**, 152–177 (2019).
- 1013 19. J. E. Hoffmann, *et al.*, Hafnium-Neodymium isotope, trace element and U-Pb
1014 zircon age constraints on the petrogenesis of the 3.44-3.46 Ga Dwalile
1015 greenstone remnant, Ancient Gneiss Complex, Swaziland. *Precambrian Res.*
1016 **351** (2020).
- 1017 20. E. Hasenstab, *et al.*, Evolution of the early to late Archean mantle from Hf-Nd-
1018 Ce isotope systematics in basalts and komatiites from the Pilbara Craton. *Earth*
1019 *Planet. Sci. Lett.* **553**, 116627 (2020).
- 1020 21. J. Blichert-Toft, N. T. Arndt, A. Wilson, G. Coetzee, Hf and Nd isotope
1021 systematics of early Archean komatiites from surface sampling and ICDP
1022 drilling in the Barberton Greenstone Belt, South Africa. *Am. Mineral.* **100**,
1023 2396–2411 (2015).
- 1024 22. M. Fischer-Gödde, *et al.*, Ruthenium isotope vestige of Earth's pre-late-veener
1025 mantle preserved in Archaean rocks. *Nature* **579**, 240–244 (2020).
- 1026 23. J. Tusch, *et al.*, Convective isolation of Hadean mantle reservoirs through
1027 Archean time. *Proc. Natl. Acad. Sci.* **118**, 1–6 (2021).
- 1028 24. J. E. Hoffmann, C. Münker, A. Polat, M. T. Rosing, T. Schulz, The origin of
1029 decoupled Hf-Nd isotope compositions in Eoarchean rocks from southern West
1030 Greenland. *Geochim. Cosmochim. Acta* **75**, 6610–6628 (2011).
- 1031 25. S. König, *et al.*, The Earth's tungsten budget during mantle melting and crust
1032 formation. *Geochim. Cosmochim. Acta* **75**, 2119–2136 (2011).
- 1033 26. A. Mundl-Petermeier, *et al.*, Temporal evolution of primordial tungsten-182 and
1034 $^3\text{He}/^4\text{He}$ signatures in the Iceland mantle plume. *Chem. Geol.* **525**, 245–259
1035 (2019).
- 1036 27. C.-L. Chou, Fractionation of siderophile elements in the earth's upper mantle.
1037 *Proc. Lunar Planet. Sci. Conf. 9th*, 219–230 (1978).
- 1038 28. U. Mann, D. J. Frost, D. C. Rubie, H. Becker, A. Audétat, Partitioning of Ru,
1039 Rh, Pd, Re, Ir and Pt between liquid metal and silicate at high pressures and
1040 high temperatures - Implications for the origin of highly siderophile element
1041 concentrations in the Earth's mantle. *Geochim. Cosmochim. Acta* **84**, 593–613
1042 (2012).
- 1043 29. S. Marchi, R. M. Canup, R. J. Walker, Heterogeneous delivery of silicate and

- 1044 metal to the Earth by large planetesimals. *Nat. Geosci.* **11**, 77–81 (2018).
- 1045 30. I. S. Puchtel, R. J. Walker, C. R. Anhaeusser, G. Gruau, Re-Os isotope
1046 systematics and HSE abundances of the 3.5 Ga Schapenburg komatiites,
1047 South Africa: Hydrous melting or prolonged survival of primordial
1048 heterogeneities in the mantle? *Chem. Geol.* **262**, 355–369 (2009).
- 1049 31. P. Waterton, J. Mungall, D. G. Pearson, The komatiite-mantle platinum-group
1050 element paradox. *Geochim. Cosmochim. Acta* (2021)
1051 <https://doi.org/10.1016/j.gca.2021.07.037>.
- 1052 32. J. M. Tucker, S. Mukhopadhyay, Evidence for multiple magma ocean
1053 outgassing and atmospheric loss episodes from mantle noble gases. *Earth*
1054 *Planet. Sci. Lett.* **393**, 254–265 (2014).
- 1055 33. R. Parai, S. Mukhopadhyay, J. J. Standish, Heterogeneous upper mantle Ne,
1056 Ar and Xe isotopic compositions and a possible Dupal noble gas signature
1057 recorded in basalts from the Southwest Indian Ridge. *Earth Planet. Sci. Lett.*
1058 **359–360**, 227–239 (2012).
- 1059 34. C. C. M. Robin-Popieul, *et al.*, A new model for barberton komatiites: Deep
1060 critical melting with high melt retention. *J. Petrol.* **53**, 2191–2229 (2012).
- 1061 35. A. W. Hofmann, Mantle geochemistry: the message from oceanic magmatism.
1062 *Nature* **385**, 219–229 (1997).
- 1063 36. J. D. Vervoort, T. Plank, J. Prytulak, The Hf-Nd isotopic composition of marine
1064 sediments. *Geochim. Cosmochim. Acta* **75**, 5903–5926 (2011).
- 1065 37. R. E. Jones, *et al.*, Origins of the terrestrial Hf-Nd mantle array: Evidence from
1066 a combined geodynamical-geochemical approach. *Earth Planet. Sci. Lett.* **518**,
1067 26–39 (2019).
- 1068 38. C. Israel, *et al.*, Formation of the Ce-Nd mantle array: Crustal extraction vs.
1069 recycling by subduction. *Earth Planet. Sci. Lett.* **530**, 115941 (2020).
- 1070 39. Hoffmann, Wilson, The origin of highly radiogenic Hf isotope compositions in
1071 3.33 Ga Comondale komatiite lavas (South Africa). *Chem. Geol.* **455**, 6–21
1072 (2017).
- 1073 40. A. Corgne, C. Liebske, B. J. Wood, D. C. Rubie, D. J. Frost, Silicate perovskite-
1074 melt partitioning of trace elements and geochemical signature of a deep
1075 perovskitic reservoir. *Geochim. Cosmochim. Acta* **69**, 485–496 (2005).
- 1076 41. A. Stracke, B. Bourdon, The importance of melt extraction for tracing mantle
1077 heterogeneity. *Geochim. Cosmochim. Acta* **73**, 218–238 (2009).
- 1078 42. C. G. Chase, P. J. Patchett, Stored mafic/ultramafic crust and early Archean
1079 mantle depletion. *Earth Planet. Sci. Lett.* **91**, 66–72 (1988).
- 1080 43. R. G. Tronnes, D. J. Frost, Peridotite melting and mineral-melt partitioning of
1081 major and minor elements at 22–24.5 GPa. *Earth Planet. Sci. Lett.* **197**, 117–
1082 131 (2002).
- 1083 44. R. Nomura, Y. Zhou, T. Irifune, Melting phase relations in the MgSiO₃–CaSiO₃
1084 system at 24 GPa. *Prog. Earth Planet. Sci.* **4** (2017).
- 1085 45. F. Nabiei, *et al.*, Investigating Magma Ocean Solidification on Earth Through

- 1086 Laser-Heated Diamond Anvil Cell Experiments. *Geophys. Res. Lett.* **48**, 1–10
1087 (2021).
- 1088 46. van K. P. E. Zegers, Middle Archean continent formation by crustal
1089 delamination. *Geology* **29**, 1083–1086 (2001).
- 1090 47. J. H. Bédard, A catalytic delamination-driven model for coupled genesis of
1091 Archean crust and sub-continental lithospheric mantle. *Geochim. Cosmochim.*
1092 *Acta* **70**, 1188–1214 (2006).
- 1093 48. T. E. Johnson, M. Brown, B. J. P. Kaus, J. A. Vantongeren, Delamination and
1094 recycling of archaean crust caused by gravitational instabilities. *Nat. Geosci.* **7**,
1095 47–52 (2014).
- 1096 49. S. Aulbach, T. Stachel, L. M. Heaman, R. A. Creaser, S. B. Shirey, Formation
1097 of cratonic subcontinental lithospheric mantle and complementary komatiite
1098 from hybrid plume sources. *Contrib. to Mineral. Petrol.* **161**, 947–960 (2011).
- 1099 50. A. L. Vesterholt, K. D. Petersen, T. J. Nagel, Mantle overturn and
1100 thermochemical evolution of a non-plate tectonic mantle. *Earth Planet. Sci.*
1101 *Lett.* **569**, 117047 (2021).
- 1102 51. J. E. Hoffmann, C. Zhang, J. F. Moyen, T. J. Nagel, “The Formation of
1103 Tonalites-Trondhjemites-Granodiorites in Early Continental Crust” in *Earth’s*
1104 *Oldest Rocks*, Second Edi, M. J. Van Kranendonk, V. C. Bennett, J. E.
1105 Hoffmann, Eds. (2019), pp. 133–168.
- 1106 52. C. Zhang, *et al.*, Constraints from experimental melting of amphibolite on the
1107 depth of formation of garnet-rich restites, and implications for models of Early
1108 Archean crustal growth. *Precambrian Res.* **231**, 206–217 (2013).
- 1109 53. W. Compston, A. Kröner, Multiple zircon growth within early Archean tonalitic
1110 gneiss from the Ancient Gneiss Complex, Swaziland. *Earth Planet. Sci. Lett.*
1111 **87**, 13–28 (1988).
- 1112 54. A. Zeh, A. Gerdes, L. Millonig, Hafnium isotope record of the Ancient Gneiss
1113 Complex, Swaziland, southern Africa: evidence for Archean crust – mantle
1114 formation and crust reworking. *J. Geol. Soc. London.* **168**, 953–963 (2011).
- 1115 55. A. Kröner, *et al.*, Generation of early Archean grey gneisses through melting
1116 of older crust in the eastern Kaapvaal craton, southern Africa. *Precambrian*
1117 *Res.* **255**, 823–846 (2014).
- 1118 56. N. Drabon, *et al.*, Heterogeneous Hadean crust with ambient mantle affinity
1119 recorded in detrital zircons of the Green Sandstone Bed, South Africa. *Proc.*
1120 *Natl. Acad. Sci. U. S. A.* **118**, 1–9 (2021).
- 1121 57. A. Mundl, R. J. Walker, J. R. Reimink, R. L. Rudnick, R. M. Gaschnig,
1122 Tungsten-182 in the upper continental crust: Evidence from glacial diamictites.
1123 *Chem. Geol.* **494**, 144–152 (2018).
- 1124 58. A. Luguet, *et al.*, Enriched Pt-Re-Os Isotope Systematics in Plume Lavas
1125 Explained by Metasomatic Sulfides. *Science (80-.)*. **319**, 453–457 (2008).
- 1126 59. M. G. Jackson, J. Blichert-toft, S. A. Halldórsson, A. Mundl-petermeier, Ancient
1127 helium and tungsten isotopic signatures preserved in mantle domains least
1128 modified by crustal recycling. *Proc. Natl. Acad. Sci.* **117**, 30993–31001 (2020).

- 1129 60. K. Burke, B. Steinberger, T. H. Torsvik, M. A. Smethurst, Plume Generation
1130 Zones at the margins of Large Low Shear Velocity Provinces on the core-
1131 mantle boundary. *Earth Planet. Sci. Lett.* **265**, 49–60 (2008).
- 1132 61. K. D. Petersen, C. Schiffer, T. Nagel, LIP formation and protracted lower
1133 mantle upwelling induced by rifting and delamination. *Sci. Rep.* **8**, 1–11 (2018).
- 1134 62. T. D. Jones, R. Maguire, P. van Keken, J. Ritsema, P. Koelemeijer, Subducted
1135 oceanic crust as the origin of seismically slow lower-mantle structures.
1136 *EarthArXiv* **1**, 1–16 (2020).
- 1137 63. T. D. Jones, D. R. Davies, P. A. Sossi, Tungsten isotopes in mantle plumes :
1138 Heads it ' s positive , tails it ' s negative. *Earth Planet. Sci. Lett.* **506**, 255–267
1139 (2019).
- 1140 64. D. M. Shaw, Trace element fractionation during anatexis. *Geochim.*
1141 *Cosmochim. Acta* **34**, 237–243 (1970).
- 1142 65. G. W. Lugmair, K. Marti, Sm-Nd-Pu timepieces in the Angra dos Reis
1143 meteorite. *Earth Planet. Sci. Lett.* **35**, 273–284 (1977).
- 1144 66. E. Scherer, C. Münker, K. Mezger, Calibration of the Lutetium-Hafnium Clock.
1145 *Science (80-.)*. **293**, 683–687 (2001).
- 1146 67. U. Söderlund, P. J. Patchett, J. D. Vervoort, C. E. Isachsen, The ¹⁷⁶Lu decay
1147 constant determined by Lu-Hf and U-Pb isotope systematics of Precambrian
1148 mafic intrusions. *Earth Planet. Sci. Lett.* **219**, 311–324 (2004).
- 1149 68. M. Tanimizu, Geophysical determination of the decay constant. *Phys. Rev. C -*
1150 *Nucl. Phys.* **62**, 4 (2000).
- 1151 69. A. Bouvier, J. D. Vervoort, P. J. Patchett, The Lu-Hf and Sm-Nd isotopic
1152 composition of CHUR: Constraints from unequilibrated chondrites and
1153 implications for the bulk composition of terrestrial planets. *Earth Planet. Sci.*
1154 *Lett.* **273**, 48–57 (2008).
- 1155 70. M. Willig, A. Stracke, Earth's chondritic light rare earth element composition:
1156 Evidence from the Ce–Nd isotope systematics of chondrites and oceanic
1157 basalts. *Earth Planet. Sci. Lett.* **509**, 55–65 (2019).
- 1158 71. F. Meissner, W. D. Schmidt-Ott, L. Ziegeler, Half-Life and alpha-Ray Energy of
1159 ¹⁴⁶Sm. *Zeitschrift für Phys.* **174**, 171–174 (1987).
- 1160 72. C. Vockenhuber, *et al.*, New half-life measurement of ¹⁸²Hf: Improved
1161 chronometer for the early solar system. *Phys. Rev. Lett.* **93**, 4–7 (2004).
- 1162 73. G. Caro, B. Bourdon, J. L. Birck, S. Moorbath, High-precision ¹⁴²Nd/¹⁴⁴Nd
1163 measurements in terrestrial rocks: Constraints on the early differentiation of the
1164 Earth's mantle. *Geochim. Cosmochim. Acta* **70**, 164–191 (2006).
- 1165 74. T. Kleine, *et al.*, Hf-W chronology of the accretion and early evolution of
1166 asteroids and terrestrial planets. *Geochim. Cosmochim. Acta* **73**, 5150–5188
1167 (2009).
- 1168 75. H. Palme, H. O'Neill, "Cosmochemical Estimates of Mantle Composition" in
1169 *Treatise on Geochemistry: Second Edition*, 2nd Ed., (Elsevier Ltd., 2014), pp.
1170 1–39.

- 1171 76. N. E. Marks, L. E. Borg, I. D. Hutcheon, B. Jacobsen, R. N. Clayton,
1172 Samarium-neodymium chronology and rubidium-strontium systematics of an
1173 Allende calcium-aluminum-rich inclusion with implications for ^{146}Sm half-life.
1174 *Earth Planet. Sci. Lett.* **405**, 15–24 (2014).
- 1175 77. T. S. Kruijer, T. Kleine, M. Fischer-Gödde, C. Burkhardt, R. Wieler,
1176 Nucleosynthetic W isotope anomalies and the Hf-W chronometry of Ca-Al-rich
1177 inclusions. *Earth Planet. Sci. Lett.* **403**, 317–327 (2014).
- 1178 78. J. Adam, T. Green, Trace element partitioning between mica- and amphibole-
1179 bearing garnet Iherzolite and hydrous basanitic melt: 1. Experimental results
1180 and the investigation of controls on partitioning behaviour. *Contrib. to Mineral.*
1181 *Petrol.* **152**, 1–17 (2006).
- 1182 79. K. N. Malitch, R. K. W. Merkle, Ru – Os – Ir – Pt and Pt – Fe alloys from the
1183 Evander Goldfield, Witwatersrand Basin, South Africa: Detrital origin inferred
1184 from compositional and Osmium-isotope data. *Can. Mineral.* **42**, 631–650
1185 (2004).
- 1186 80. M. L. G. Tejada, *et al.*, Cryptic lower crustal signature in the source of the
1187 Ontong Java Plateau revealed by Os and Hf isotopes. *Earth Planet. Sci. Lett.*
1188 **377–378**, 84–96 (2013).
- 1189 81. A. V. Sobolev, *et al.*, The Amount of Recycled Crust in Sources of Mantle-
1190 Derived Melts. *Science (80-.)*. **316**, 412–418 (2007).
- 1191 82. W. L. Griffin, *et al.*, The Hf isotope composition of cratonic mantle: LAM-MC-
1192 ICPMS analysis of zircon megacrysts in kimberlites. *Geochim. Cosmochim.*
1193 *Acta* **64**, 133–147 (2000).
- 1194 83. J. E. Hoffmann, *et al.*, Mechanisms of Archean crust formation inferred from
1195 high-precision HFSE systematics in TTGs. *Geochim. Cosmochim. Acta* **75**,
1196 4157–4178 (2011).
- 1197 84. H. Becker, Re-Os fractionation in eclogites and blueschists and the implications
1198 for recycling of oceanic crust into the mantle. *Earth Planet. Sci. Lett.* **177**, 287–
1199 300 (2000).
- 1200 85. J. A. Lewis, *et al.*, Sulfur isotope evidence for surface-derived sulfur in
1201 Eoarchean TTGs. *Earth Planet. Sci. Lett.* **576**, 117218 (2021).
- 1202 86. K. Righter, E. H. Hauri, Compatibility of rhenium in garnet during mantle
1203 melting and magma genesis. *Science (80-.)*. **280**, 1737–1741 (1998).
- 1204 87. W. Van Westrenen, J. D. Blundy, B. J. Wood, Effect of Fe^{2+} on garnet-melt
1205 trace element partitioning: experiments in FCMAS and quantification of crystal-
1206 chemical controls in natural systems. *Lith* **53**, 189–201 (2000).
- 1207 88. J. M. Brenan, C. F. Finnigan, W. F. McDonough, V. Homolova, Experimental
1208 constraints on the partitioning of Ru, Rh, Ir, Pt and Pd between chromite and
1209 silicate melt: The importance of ferric iron. *Chem. Geol.* **302–303**, 16–32
1210 (2012).
- 1211 89. S. B. Shirey, R. J. Walker, The Re-Os isotope system in cosmochemistry and
1212 high-temperature geochemistry. *Annu. Rev. Earth Planet. Sci.* **26**, 423–500
1213 (1998).

- 1214 90. M. Tatsumoto, R. J. Knight, C. J. Allegre, Time differences in the formation of
1215 meteorites as determined from the ratio of lead-207 to lead-206. *Science* (80-
1216). **180**, 1279–1283 (1973).
- 1217 91. F. Albarède, A. Michard, Transfer of continental Mg, S, O and U to the mantle
1218 through hydrothermal alteration of the oceanic crust. *Chem. Geol.* **57**, 1–15
1219 (1986).
- 1220 92. B. S. Kamber, The evolving nature of terrestrial crust from the Hadean, through
1221 the Archaean, into the Proterozoic. *Precambrian Res.* **258**, 48–82 (2015).
- 1222 93. B. S. Kamber, S. Moorbath, Initial Pb of the Amitsoq gneiss revisited:
1223 Implication for the timing of early Archaean crustal evolution in West
1224 Greenland. *Chem. Geol.* **150**, 19–41 (1998).
- 1225 94. S. Moorbath, H. Welke, N. H. Gale, The significance of lead isotope studies in
1226 ancient, high-grade metamorphic basement complexes, as exemplified by the
1227 Lewisian rocks of Northwest Scotland. *Earth Planet. Sci. Lett.* **6**, 245–256
1228 (1969).
- 1229 95. D. Wilton, Metallogenic and tectonic implications of Pb isotope data for galena
1230 separates from the Labrador Central Mineral Belt. *Econ. Geol.* **86**, 1721–1736
1231 (1991).
- 1232 96. H. S. C. O'Neill, A. J. Berry, S. M. Eggins, The solubility and oxidation state of
1233 tungsten in silicate melts: Implications for the comparative chemistry of W and
1234 Mo in planetary differentiation processes. *Chem. Geol.* **255**, 346–359 (2008).
- 1235 97. R. O. C. Fonseca, *et al.*, Redox controls on tungsten and uranium
1236 crystal/silicate melt partitioning and implications for the U/W and Th/W ratio of
1237 the lunar mantle. *Earth Planet. Sci. Lett.* **404**, 1–13 (2014).
- 1238 98. M. M. Thiemens, P. Sprung, R. O. C. Fonseca, F. P. Leitzke, C. Münker, Early
1239 Moon formation inferred from hafnium–tungsten systematics. *Nat. Geosci.* **12**
1240 (2019).
- 1241 99. C. Schnabel, C. Münker, E. Strub, La-Ce isotope measurements by
1242 multicollector-ICPMS. *J. Anal. At. Spectrom.* **32**, 2360–2370 (2017).
- 1243 100. A. Makishima, E. Nakamura, Precise measurement of cerium isotope
1244 composition in rock samples. *Chem. Geol.* **94**, 1–11 (1991).
- 1245 101. M. Willbold, Determination of Ce isotopes by TIMS and MC-ICPMS and
1246 initiation of a new, homogeneous Ce isotopic reference material. *J. Anal. At.*
1247 *Spectrom.* **22**, 1364–1372 (2007).
- 1248 102. J. Völkening, M. Köppe, K. G. Heumann, Tungsten isotope ratio determinations
1249 by negative thermal ionization mass spectrometry. *Int. J. Mass Spectrom. Ion*
1250 *Process.* **107**, 361–368 (1991).

1251

1252

1253

1254

SI Appendix

Geological background of our sample selection

We analyzed a comprehensive set of rocks from the Kaapvaal Craton that range from different types of grey orthogneisses (TTGs and more evolved granitoids) to mantle-derived lithologies of mafic-ultramafic composition. This representative suite of 17 samples span an age range from 3.55 to 3.22 Ga and represent the main lithological units of the Ancient Gneiss Complex (AGC), also comprising the oldest mafic rocks (lower Onverwacht Group, 3.55 to 3.45 Ga) of the Barberton Granite-Greenstone Terrane (BGGT).

The AGC is located in Swaziland and is a typical high-grade gneiss terrain that comprises 3.66-3.20 Ga old rocks(103). The oldest part of the AGC are polydeformed granitoid gneisses, heterogeneous in age and composition(55, 104), that are interbanded with amphibolites. Together, they formed layered grey gneiss sequences in response to ductile deformation under high strain conditions(103). The different varieties of rocks from this sequence have been summarized as the Ngwane Gneiss (NG)(105). The oldest generation of NG (*NG sensu stricto*) are 3.66 Ga to 3.5 Ga granitoid gneisses(53–55, 104, 106) that mainly belong to the tonalite-trondhjemite-granodiorite (TTG) suite but also comprise granitic rocks. As indicated by trace element systematics(53), whole rock Nd isotope systematics(107) and Hf-in-zircon isotope data(53–55) the protoliths of the orthogneisses resulted, at least in part, from melting of a LREE enriched source with considerable residence time, most likely older continental crust of Eoarchean to late Hadean age. Younger generations of grey gneisses, which are mapped as NG, were emplaced after 3.45 Ga. These show the same field appearance as the 3.66-3.45 Ga NG but are as young as 3.2 Ga(107, 108). The oldest NG hosts scattered remnants of supracrustal assemblages with greenstone belts (e.g. Dwalile Supracrustal Suite, DSS(109)). These remnants postdate the oldest NG, vary in size and are either infolded, occur as tectonically intercalated xenoliths of a few centimeters or even represent coherent blocks of several kilometers(109, 110). The origin of these remnants remains contentious. They were interpreted either as strongly flattened dikes(109, 111) or as dismembered portions of the Dwalile Greenstone Remnant (DGR), which represents the largest of the greenstone remnants of the AGC(55, 103, 110, 112). The DGR is located in SW Swaziland and the supracrustal rock assemblage (metavolcanics, metasediments) were shown to be extruded between 3.44 and 3.46 Ga, therefore postdating the oldest generation of NG(19, 110, 113). Notably, the metavolcanic rocks from the DGR share geochemical similarities with volcanic assemblages from the Onverwacht Group which hints at a genetic link between the DGR and the BGGT(19, 110, 111). Based on trace element systematics and variable whole-rock initial ϵNd and ϵHf values it has been argued that the mafic and ultramafic DGR rocks were derived from a mildly depleted mantle source and were in part contaminated by rocks from an ancient continental source, presumably crustal material of NG-like composition(19, 110). The oldest NG and intercalated members of the DSS were intruded by the texturally and compositionally distinct Tsawela Gneiss between 3.48-3.43 Ga(54, 108, 109, 114, 115) and younger generations of grey gneisses that date back to ca. 3.2 Ga(108).

All sample localities are shown in SI Appendix, Fig. S13 and GPS coordinates are provided in previous studies(18, 55, 112, 114). We have analyzed two grey gneisses

from the >3.45 Ga NG suite that were collected along the Mtimane River in the Mankayane area in central Swaziland, where granitoid gneisses of different ages were variably affected by intensive regional migmatization at ca. 3.2 Ga(110, 116, 117). Both samples (AGC 351 and AGC 352) were previously described(55, 114). AGC 351 is a 3.455 Ga old, strongly migmatized grey gneiss of near granitic composition and interpreted to be derived from felsic crustal precursors that mixed with juvenile, depleted mantle-derived melts(55, 116). AGC 352 is a 3.442 Ga very homogeneous fine grained grey gneiss(114).

We have analyzed several samples from greenstone remnants that are interlayered with grey gneisses of the AGC. We investigated two komatiites and one amphibolite from the DGR (AGC 83, AGC 86 and AGC 38), one typical amphibolite fragment as found in the AGC (AGC 222) and a 3.455 Ga gabbroic enclave (AGC 350) from central Swaziland. The mafic-ultramafic rock samples from the DGR were previously characterized(19, 110). Sample AGC 222 is a fragmented amphibolite enclave from Kubuta in central Swaziland with a minimum age of 3.4 Ga(118). It is similar in composition to other greenstone remnants found in the AGC(55, 114). Gabbroic enclaves like AGC 350 can be found along the Mtimane River in the Mankayane area close to the sample localities of AGC 351 and AGC 352. As described by reference (116) the precursors of the gabbroic enclaves were emplaced together with granitoid gneisses at 3.455 Ga. At about 3.2 Ga, a tectono-magmatic-metamorphic event reworked the grey gneisses and greenstones(117) which led to boudinage and local anatexis of the gabbros and migmatization of the grey gneisses (e.g. sample locality of AGC 351).

The youngest samples from the AGC are two ca. 3.2 Ga gneisses. Sample AGC 473 is a 3.24 Ga grey gneiss of trondhjemitic composition, which intruded into the oldest generation of NG northwest of the DGR. Based on structural considerations, the adjacent NG were interpreted as basement for the volcanic sequences of the DGR(109). Our younger grey gneiss sample AGC 473 belongs to the youngest generation of NG but contains inherited zircon grains of 3.49 Ga and ca. 3.64 Ga(15). This young generation of grey gneisses belongs to a 3.2 Ga magmatic event that is typically associated with indicators for strong deformation and high-grade metamorphism and therefore suggested to be the result of migmatization and crustal melting of older generations of crustal rocks(112, 116). Sample AGC 445 is a 3.216 Ga old grey gneiss from the Piggs Peak area also belonging to the former 3.2 Ga NG generation(112).

The AGC is in faulted contact with the BGGT along the ca. > 3.2 Ga old Phophonyane shear zone northwest of Pigg's Peak town(106) and is spatially separated by sheet-like intrusions of the Mpuluzi and Piggs Peak batoliths. Rocks from the BGGT comprise a complex association of greenstone sequences and grey gneisses. The greenstone sequences in the BGGT (referred to as the Barberton Greenstone Belt, BGB) comprise a complex association of volcanic-sedimentary rocks that were deposited over more than 300 million years from < 3547 to > 3219 Ga(119). The volcano-sedimentary sequence of the BGB (known as the Barberton Supergroup) has traditionally been divided (from base to top) into three main lithostratigraphic units: The Onverwacht, Fig Tree, and Moodies groups. The Onverwacht Group (OG) is the oldest greenstone succession of the BGB and comprises voluminous mafic to ultramafic metavolcanics

successions with sparsely interbedded metasediments. As we only analyzed samples from the lower OG, we only provide a short overview about the lowest stratigraphy of the BGB. The OG is subdivided into the lower and upper Onverwacht Group, marked by a chert layer, known as the Middle Marker. The lower OG comprises the Sandspruit, Theespruit, and Komati Formations, the upper OG includes the Hoggenoeg, Noisy, Mendon, and Kromberg Formations(120). The oldest magmatic events preserved in the lithostratigraphic succession of the BGB are mafic-ultramafic and felsic metavolcanic rocks. This bimodal sequence (originally assigned to the Sandspruit and Theespruit Formations) comprises the oldest rocks of the lower Onverwacht Group. The metavolcanic rocks of the Sandspruit and Theespruit Formations were shown to be time-equivalent and deposited during one single volcanic event at ca. 3530 Ma and therefore constitute a single lithostratigraphic unit(121). The record of the somewhat younger 3.482 Ga Komati Formation(120) bears witness to a period of prolonged volcanic activity, as it comprises a continuous succession of alternating komatiitic, komatiitic basalt, and tholeiitic basalt lava flows without any intercalated sedimentary layers that would reflect a hiatus in the stratigraphy(122).

The BGB is surrounded by 3.521 to 3.197 Ga old granitoid gneisses(112) that form a cluster of 12 diapiric plutons with a wide variety of compositional types that intruded into the lowermost formations of the BGB(123). They can be subdivided into two major compositionally families that were emplaced during two periods: The older (3.45-3.2 Ga) TTG group that was coeval with deposition of supracrustal sequences in the BGB, and the much younger (ca. 3.1 Ga) GMS group (granite-monzonite-syenite) which intruded after sedimentation and stabilization of the crust through continued deformation of the TTG basement and greenstone sequences at ca. 3.2 Ga(119).

Our samples were collected at the southwestern margin of the BGGT southeast of the town of Badplaas, in an area around the settlement of Tjakastad (SI Appendix, Fig. S13). Here a significant proportion of the metavolcanic rocks from the Sandspruit and Theespruit Formations occur as dismembered rafts and xenoliths in tonalitic-trondhjemitic gneisses of the Badplaas, Stolzburg and Theespruit Plutons in the southern part of the Barberton Mountain Land(123, 124).

In order to better understand the depletion history of the Kaapvaal Craton we also investigated ultramafic rocks from the Komati Formation sampled from the BARB1 and BARB2 drillcores that were dragged during an International Continental Drilling Program (ICDP-2009/01, Exp.ID 5047) in the Onverwacht Group of the BGB(125). The exact core-positions of the samples analyzed are provided in Table S2.

Supplementary Figures

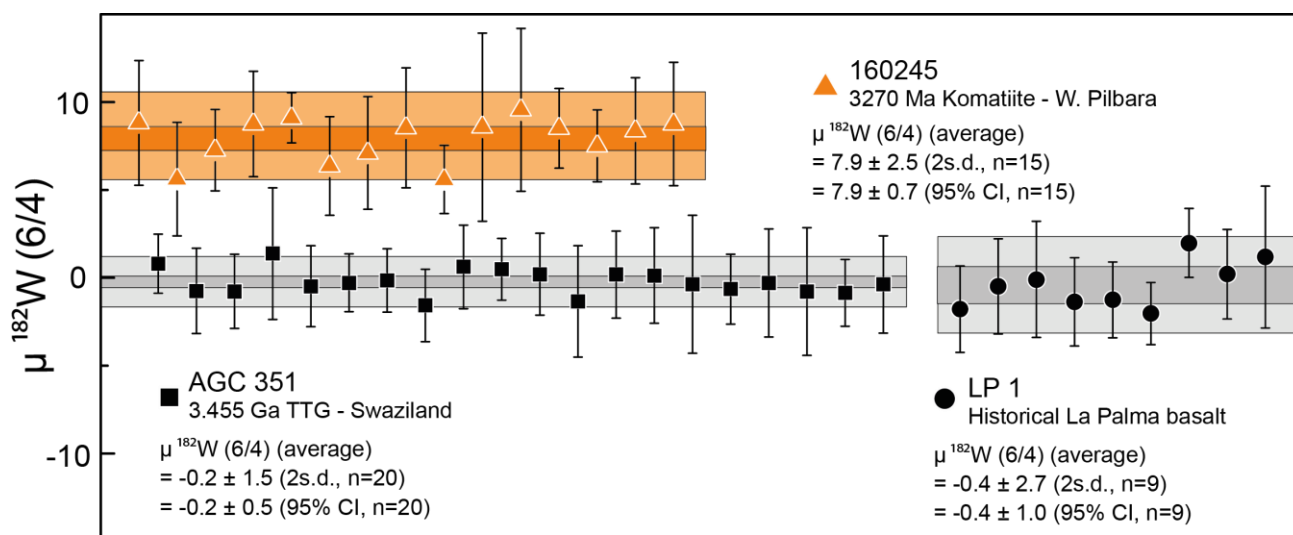
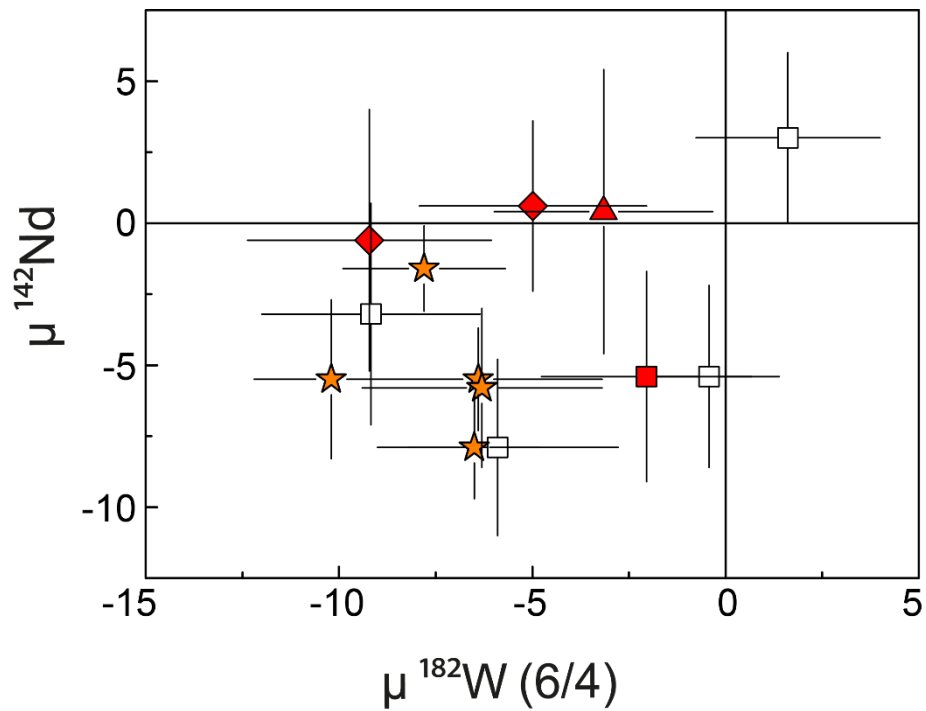


Fig. S1: Intermediate precision for $\mu^{182}\text{W} (6/4)$, inferred from the repeated analysis of multiple digestions for our in – house reference materials AGC 351, LP 1, and 160245 that are reported relative to W NIST SRM 3136. Each symbol refers to the average value of multiple measurements conducted during an analytical session. The uncertainties for the session mean values are given by the corresponding 95% CI. The intermediate precision for our in–house reference materials are given by the 2 SD of the session mean values.



This study

Previous study¹²

■ Komati

▲ Sandspruit

◆ Others

□

— Mantle derived —

★ Schapenburg

— Granitoids

Fig. S2: Compilation of available $\mu^{182}\text{W}$ and $\mu^{142}\text{Nd}$ for crustal and mantle-derived rocks from the Kaapvaal Craton. Symbols for our samples are the same as in Fig. 1. The ^{142}Nd isotope compositions for samples from our study were previously reported(15) and combined $^{182}\text{W} - ^{142}\text{Nd}$ systematics for komatiites from the Schapenburg Greenstone Remnant (SGR) were taken from the literature(12). The combined data show a tendency towards negative anomalies but reveal no clear correlation due to the comparatively large uncertainties.

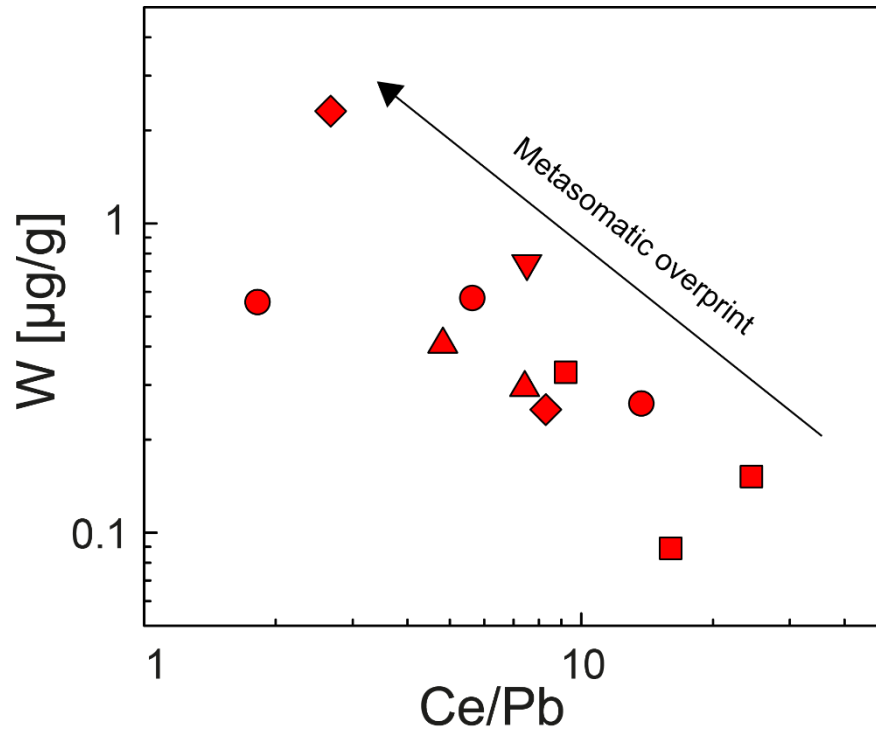


Fig. S3: Compositions of W (μg/g) vs. Ce/Pb as an indicator for selective W mobility by metasomatic fluids. Symbols are the same as in Fig. 1.

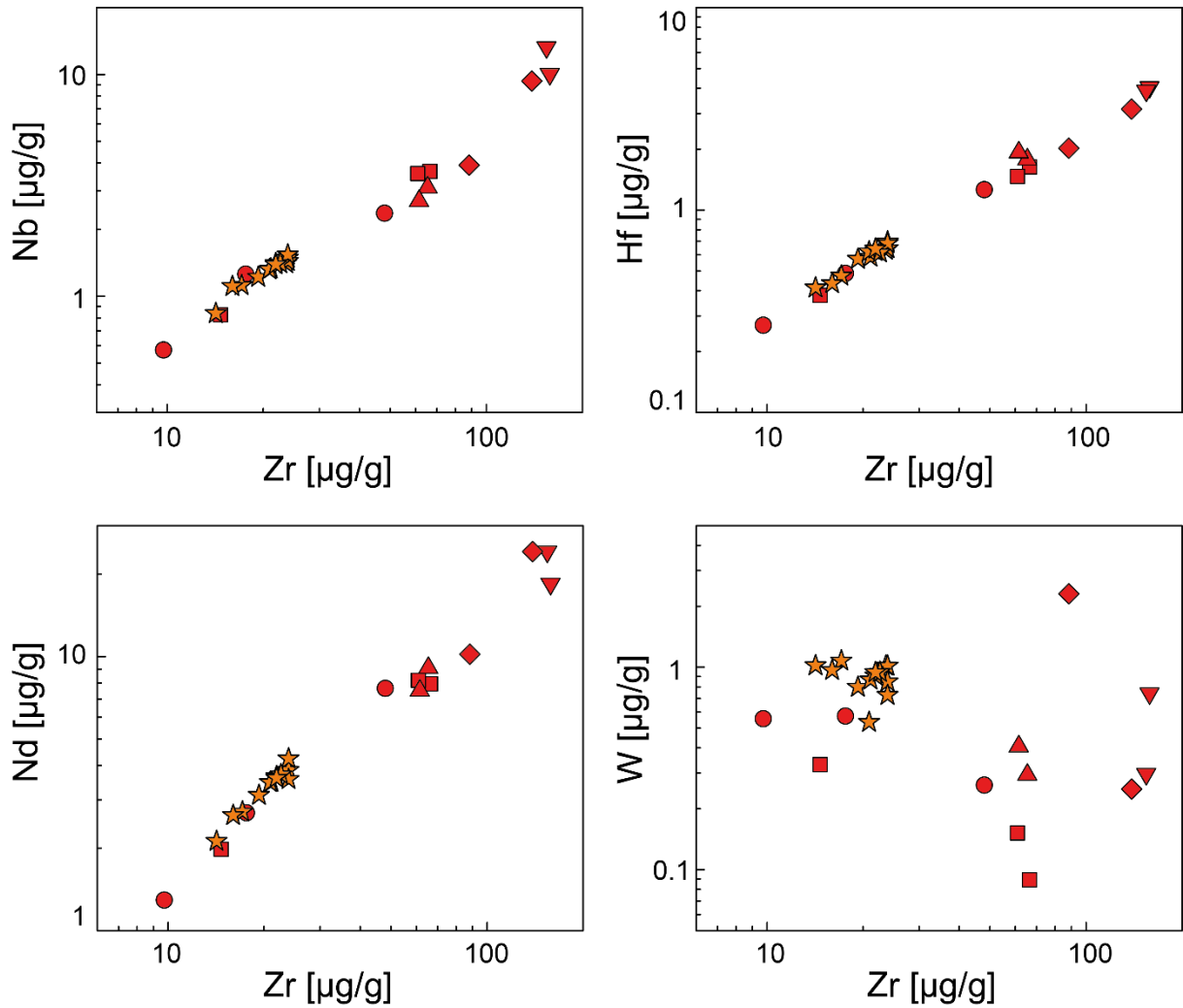


Fig. S4: Trace element variation diagrams [$\mu\text{g/g}$] of Nb, Hf, Nd, and W vs. Zr-content for our samples and the Schapenburg komatiite suite⁽¹²⁾. The positive correlations of incompatible elements (e.g. Nb, Nd, Hf) in variation diagrams vs. Zr content reveal that HFSE and REE were not affected by metasomatic processes. In contrast, no primary magmatic differentiation trends are preserved for W.

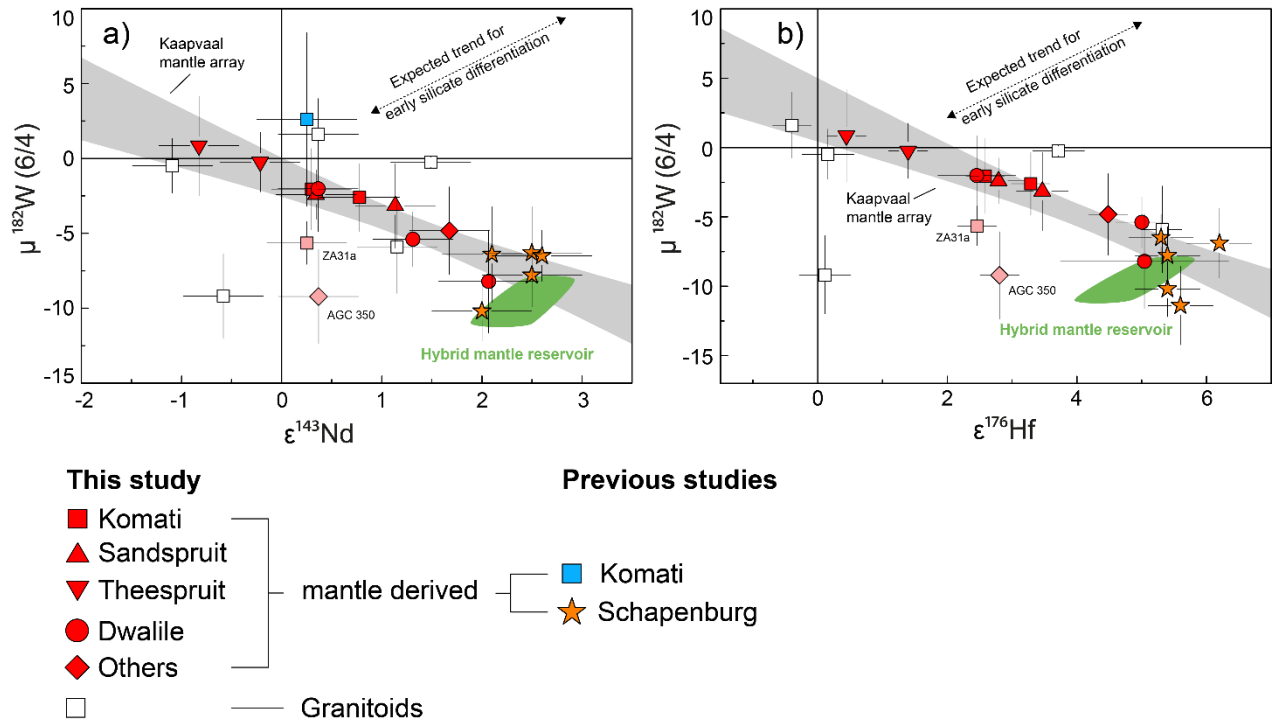


Fig. S5: Measured $\mu^{182}\text{W}$ vs. $\epsilon^{143}\text{Nd}_{(t)}$ (a) and $\mu^{182}\text{W}$ vs. $\epsilon^{176}\text{Hf}_{(t)}$ (b) for mantle-derived and TTG-like mafic rock samples from the Kaapvaal Craton including literature data. The literature data include previously published data for komatiites from the Schapenburg Greenstone Remnant (orange asterisks)(12) and the Komati Formation (blue square)(11, 16). We note that previously published literature data for the Komati Formation only report combined $\mu^{182}\text{W}$ vs. $\epsilon^{143}\text{Nd}_{(t)}$ data for one single sample (sample BV 02, blue square)(11,16). The green fields illustrate modeled values of our proposed hybrid reservoir (10-20% restites admixed to depleted mantle). The shaded grey field, referred to as Kaapvaal mantle array, is an uncertainty envelope employing the 95% confidence interval in which of all mantle-derived samples are expected to fall. Note, that the negative co-variation displayed by the Kaapvaal mantle array does not follow the expected trend for early silicate differentiation (indicated by dashed line in panel b).

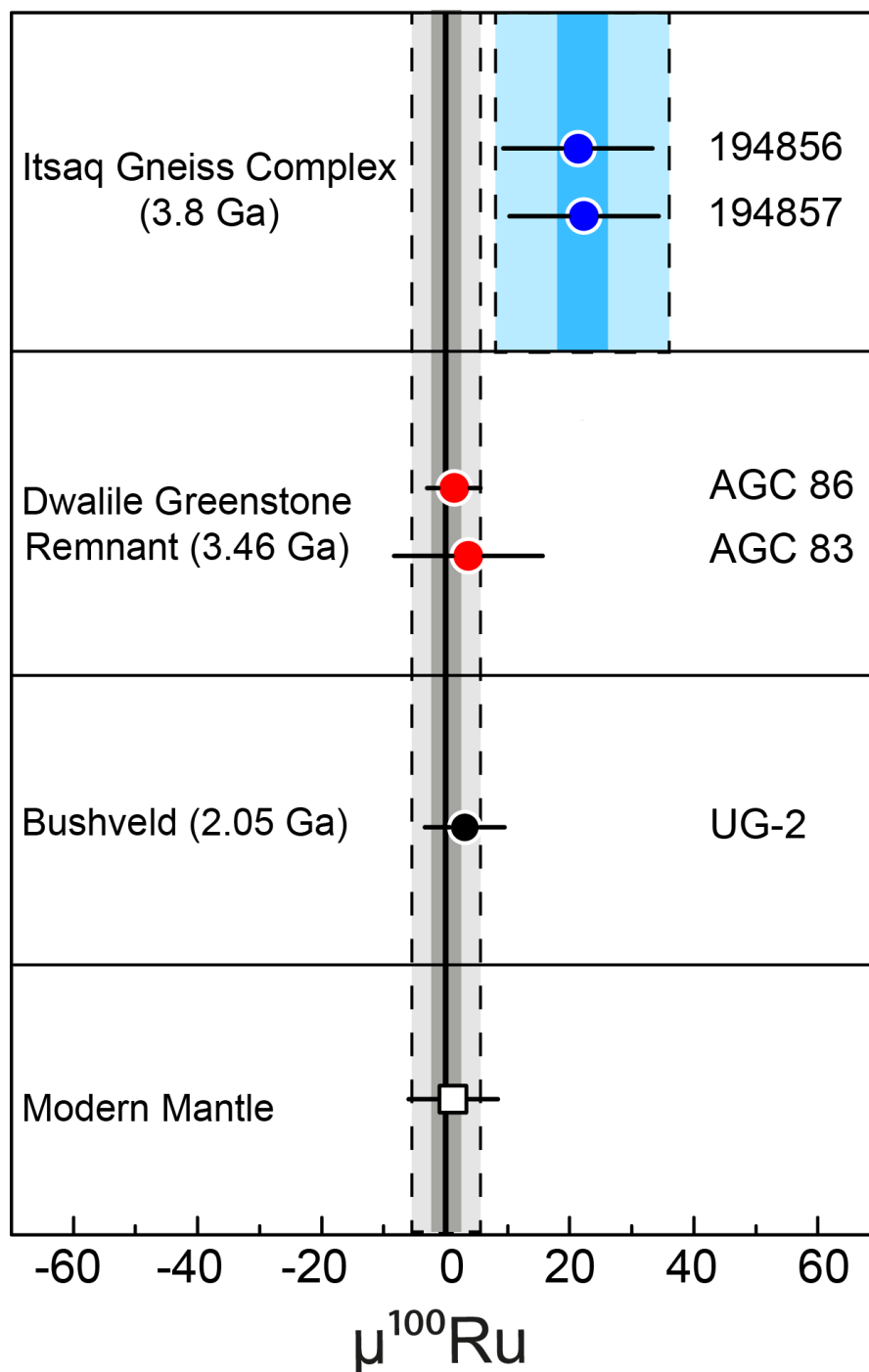


Fig. S6: $\mu^{100}\text{Ru}$ data for Archean and Palaeoproterozoic rocks measured in this study and a previous publication(22) compared to the modern mantle(126). Uncertainties for individual data points either refer to the external uncertainty of the method (2.s.d. for samples measured $n < 4$ times) or involve the corresponding 95% confidence interval of the repeated analysis of a given sample (if $n \geq 4$). The grey and blue bars represent the previously reported range for the modern mantle and Eoarchean mantle rocks from the Itsaq gneiss complex (22). Dark and bright shaded colors indicate the 2 s.d. uncertainty of the mean and the respective 95% confidence interval, respectively. The chromitite samples from the Itsaq gneiss complex (194856 & 194857, blue symbols) and the Bushveld igneous province (UG-2, black symbol) that were measured in this study are in accord with previous results that found anomalous and modern mantle-like $\mu^{100}\text{Ru}$ isotope compositions, respectively. Komatiites from the Dwalile greenstone remnant (AGC 83 & AGC 86, red symbols) reveal no resolvable $\mu^{100}\text{Ru}$ isotope anomalies.

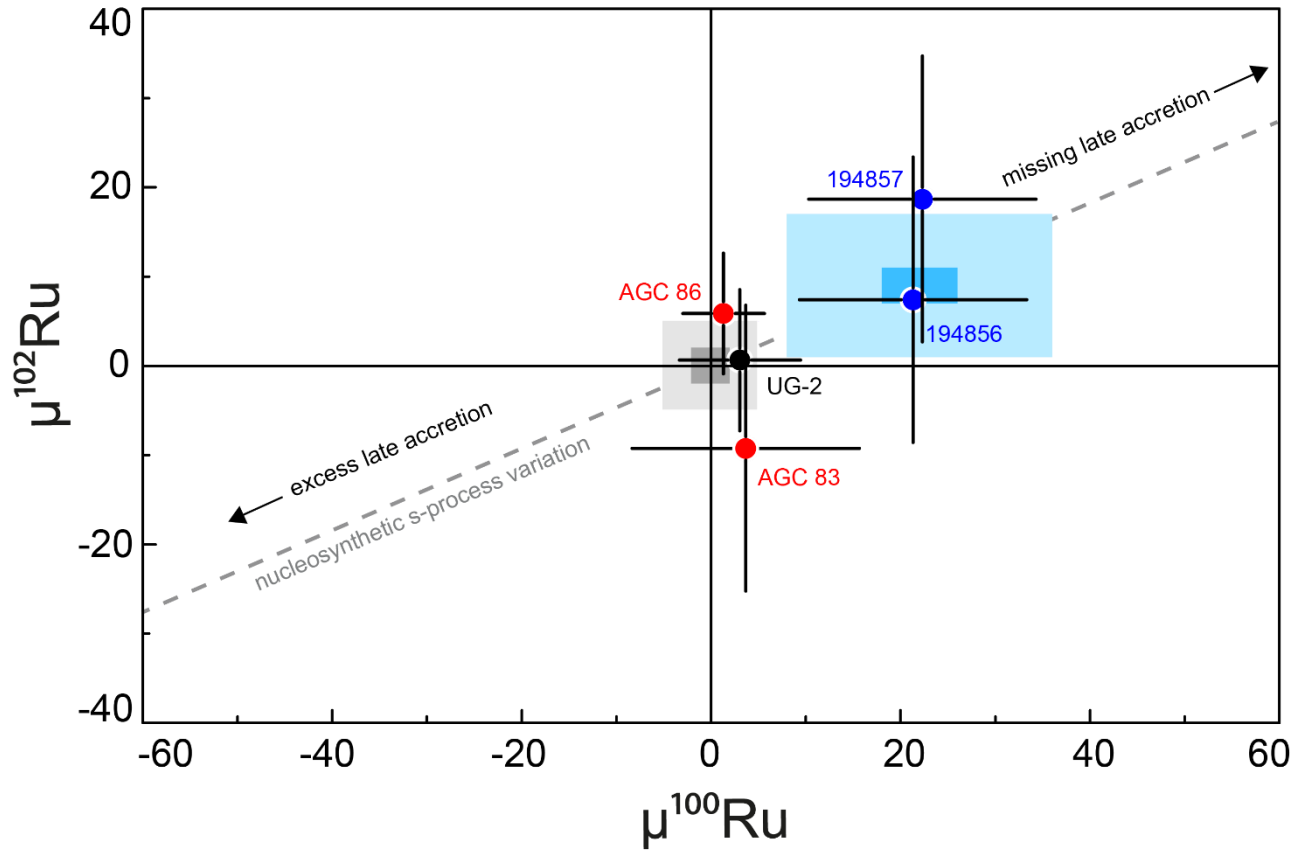


Fig. S7: Ru isotope plot illustrating the effect of heterogeneous late accretion on the Ru isotope composition in terrestrial rocks. The uncertainties for individual data points, the modern mantle (grey box) and the Eoarchean mantle in the Itsaq gneiss complex (blue box) are the same as in Fig. S6. The dashed line illustrates mixing relationships between the modern mantle composition and primitive material that has been shown to exhibit Ru isotope systematics that carry a signature of s-process nucleosynthetic composition(127). As demonstrated for Eoarchean mantle rocks from the Itsaq gneiss complex (SW Greenland) coupled $\mu^{100}\text{Ru}$ - $\mu^{102}\text{Ru}$ isotope systematics in terrestrial rocks can serve as a tool to investigate to which extend mantle reservoirs equilibrated with late accreted material(22). The coupled $\mu^{100}\text{Ru}$ - $\mu^{102}\text{Ru}$ isotope systematics for komatiites from the Dwalile greenstone remnant (AGC 83 & AGC 86, red symbols) overlap with the modern mantle composition and do not indicate that their mantle sources carried excess late accreted material or did not fully equilibrated with late accreted material.

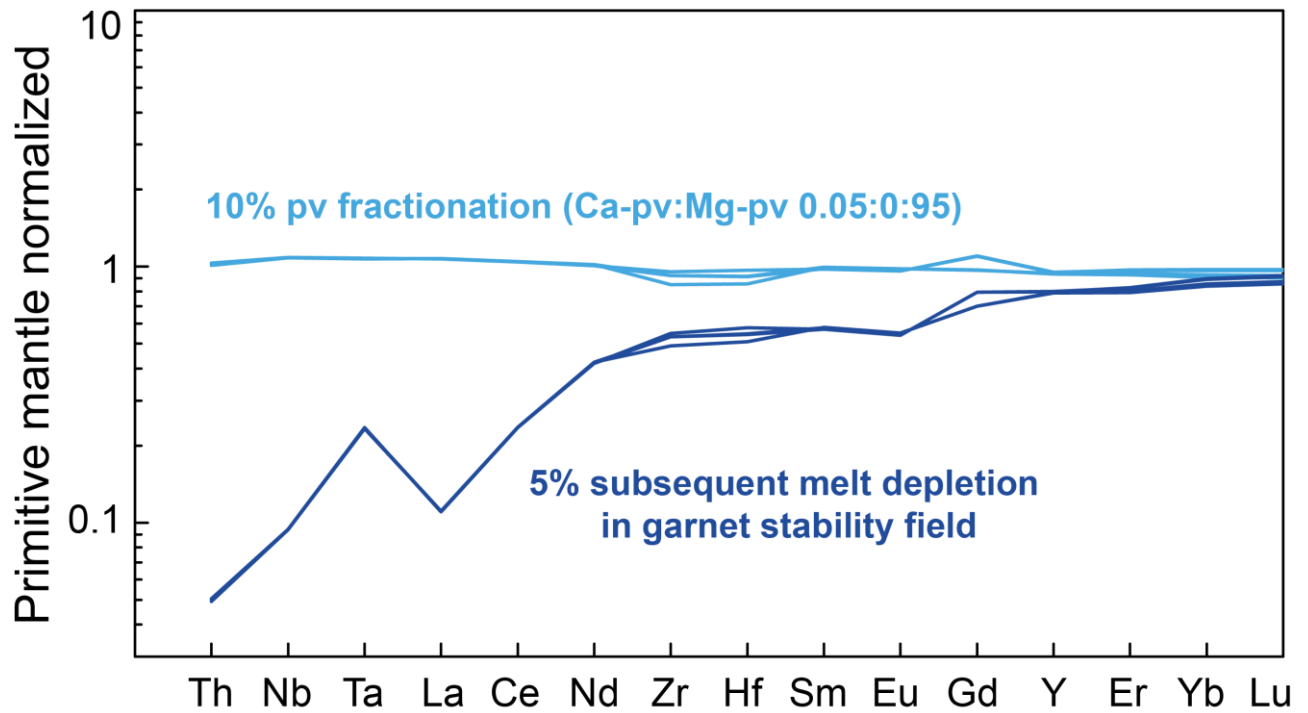


Fig. S8: Incompatible trace element compositions for primitive mantle that undergoes removal of 10% perovskite (pale blues patterns) before it undergoes batch melting in the garnet stability field (dark blue patterns). The removal of 10% perovskite does not lead to fractionated trace element patterns that are expected to explain the radiogenic initial ^{176}Hf - ^{143}Nd compositions in Kaapvaal Craton rocks (Figs 3 and S11). Rather, subsequent melt depletion in the garnet stability field significantly affects the incompatible trace element budget and generates the observed ^{176}Hf - ^{143}Nd systematics. Note that different lines for both reservoirs result from slight differences in perovskite partition coefficients for experimental charges(40).

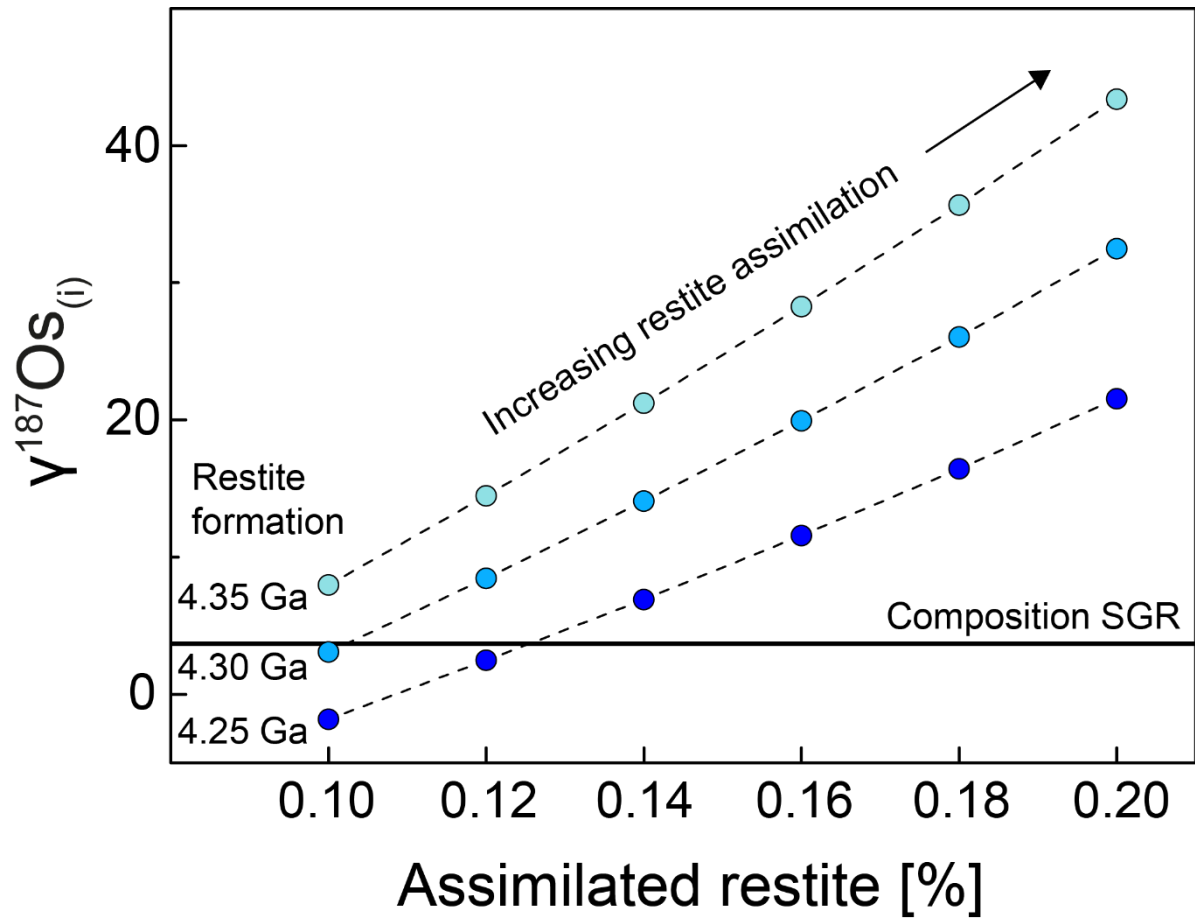


Fig. S9: Modelled $\gamma^{187}\text{Os}$ compositions for hybrid mantle reservoirs comprising depleted mantle and residual restites. Shown are modelled initial $\gamma^{187}\text{Os}$ compositions for depleted mantle that assimilated 10-20% residual restites. Following the time evolution path of our model we show mixing relationships for three generations of residual restites that formed during TTG formation between 4.35 Ga and 4.25 Ga. For explanation see method section. Calculations can be followed in Table S3.

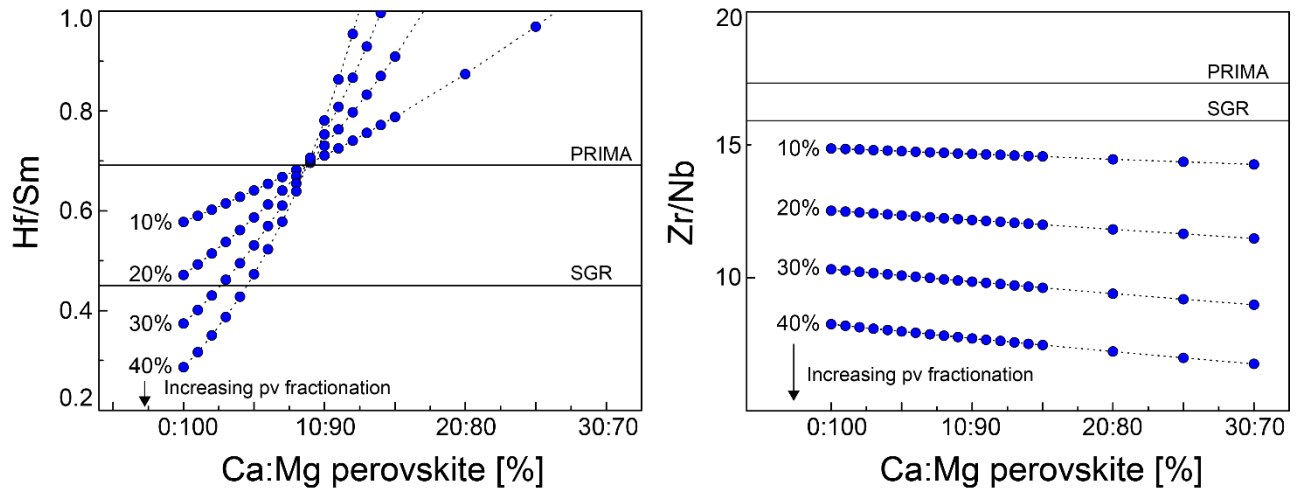


Fig. S10: Modelled effects on ratios of (a) Hf/Sm and (b) Zr/Nb in a primitive mantle like reservoir that underwent removal of different Ca-Mg perovskite assemblages, considering different Ca-Mg perovskite proportions and various degrees of perovskite fractionation. (a) The effect of Ca-Mg perovskite proportions on Hf/Sm illustrates that Ca-perovskite fractionates many trace elements in the opposite manner as Mg-perovskite, a fact that is frequently overlooked when investigating trace element ratios that behave sensitive to perovskite fractionation. **(b)** Rather, trace element ratios should be used that are largely insensitive to the choice of Ca-Mg perovskite proportions (e.g. Zr/Nb).

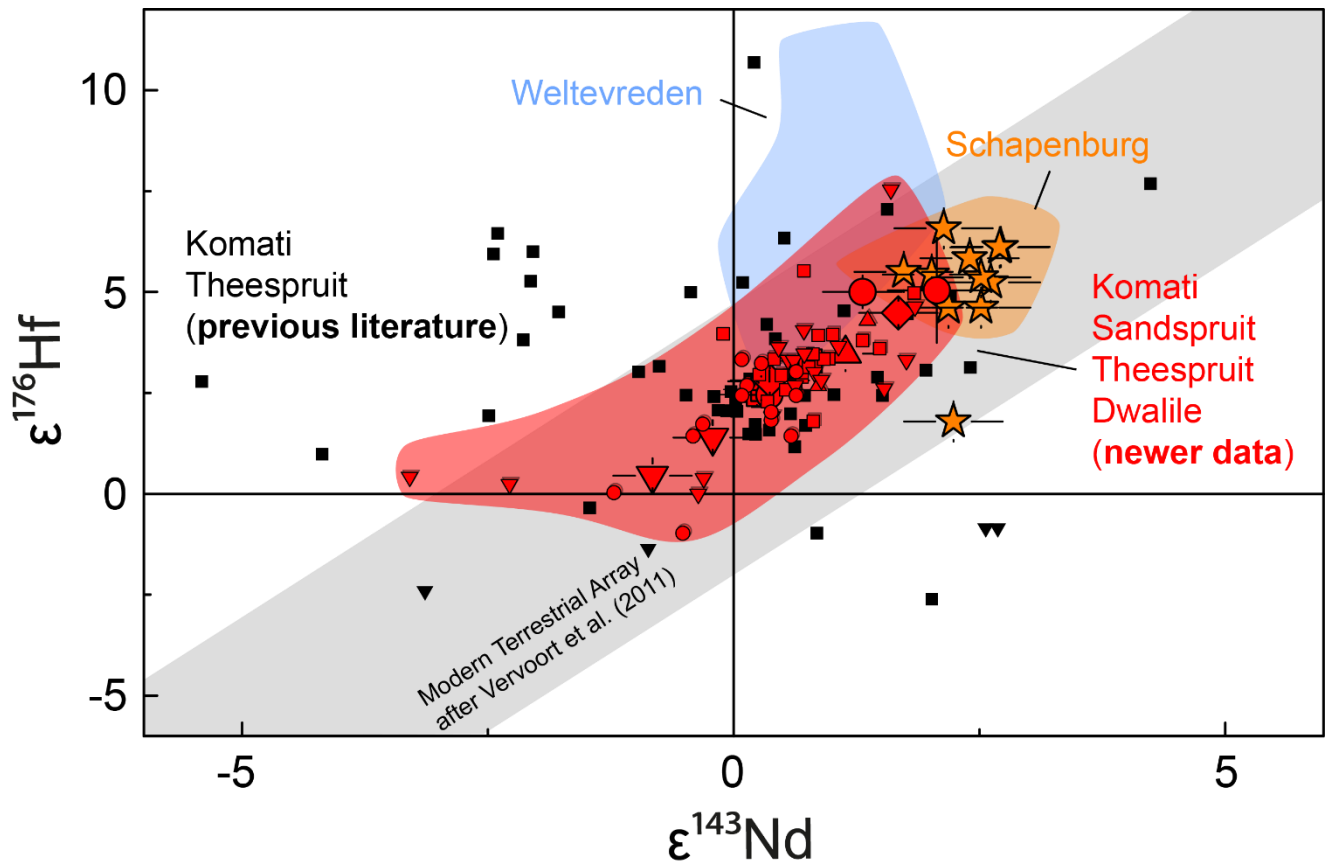


Fig. S11: $\epsilon^{176}\text{Hf}_{(t)}$ vs. $\epsilon^{143}\text{Nd}_{(t)}$ diagram for mantle-derived mafic-ultramafic rocks from this and previous studies. Symbols for our samples are the same as in Fig. 1. Previous literature data from the Komati and Theespruit Formations are displayed by black symbols(16, 21, 128-130). Newer data (red symbols) are taken from more recent studies(18, 19) and are the data source for samples analyzed in this study (large red symbols). Note that newer data for the Komati formation also comprises ultramafic samples from drillcores BARB1 and BARB2 (analyzed in this study) that significantly scatter in previous datasets. The orange field is defined by komatiites from the Schapenburg Greenstone Remnant (orange stars)(12, 131, 132). The blue field shows the array for the Weltevreden komatiite suite(16, 21). The grey bar shows the Modern Terrestrial Array for MORBs and OIBs ($\epsilon\text{Hf} = 1.55 \times \epsilon\text{Nd} + 1.21$)(36).

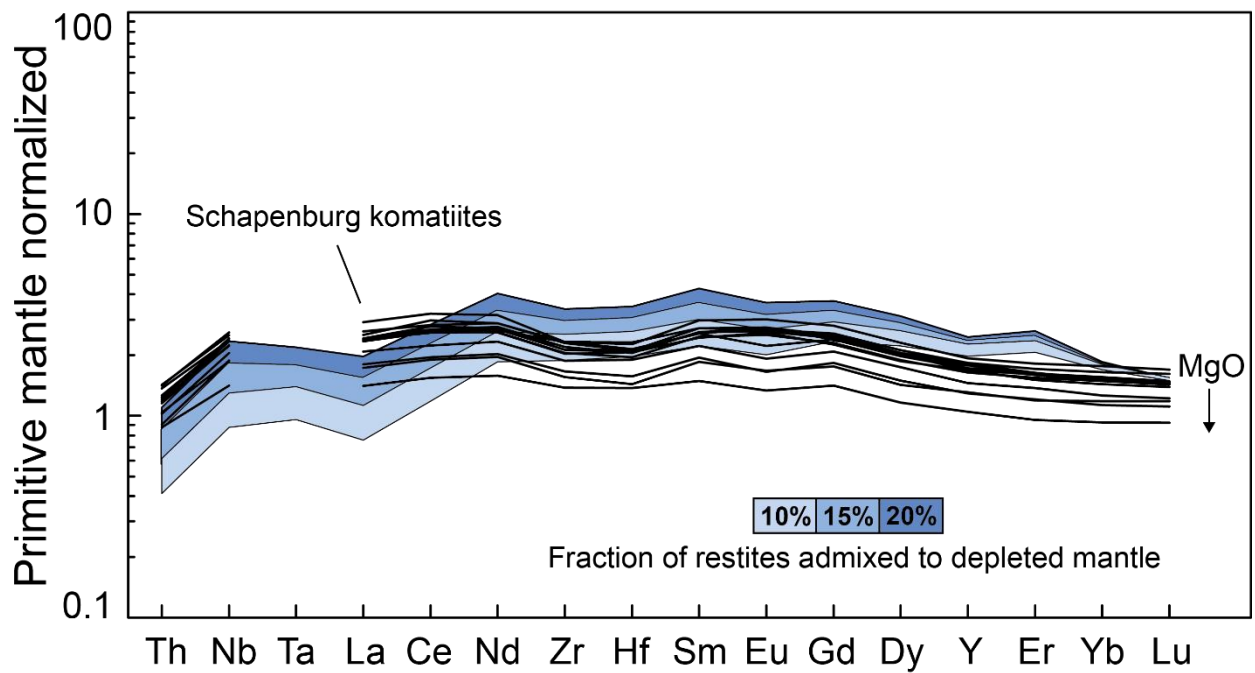


Fig. S12: Incompatible trace element compositions for komatiites from the Schapenburg Greenstone Remnant (black lines) in comparison to melts generated from our modeled hybrid sources (blue shaded arrays). Data for the SGR komatiites are taken from the literature(12). In our model calculations 10 – 20 % of garnet – rich lower crustal restite admixed to a depleted mantle at 3.55 Ga and subsequent 20 – 30% batch melting of this hybrid source can reproduce the trace element compositions of the SGR komatiites. As outlined previously (12,30) we attribute the variation within the SGR komatiite suite and their more depleted trace element compositions, compared to the modeled patterns, to olivine accumulation as indicated by co-variations between MgO content and incompatible trace element concentrations (not shown).

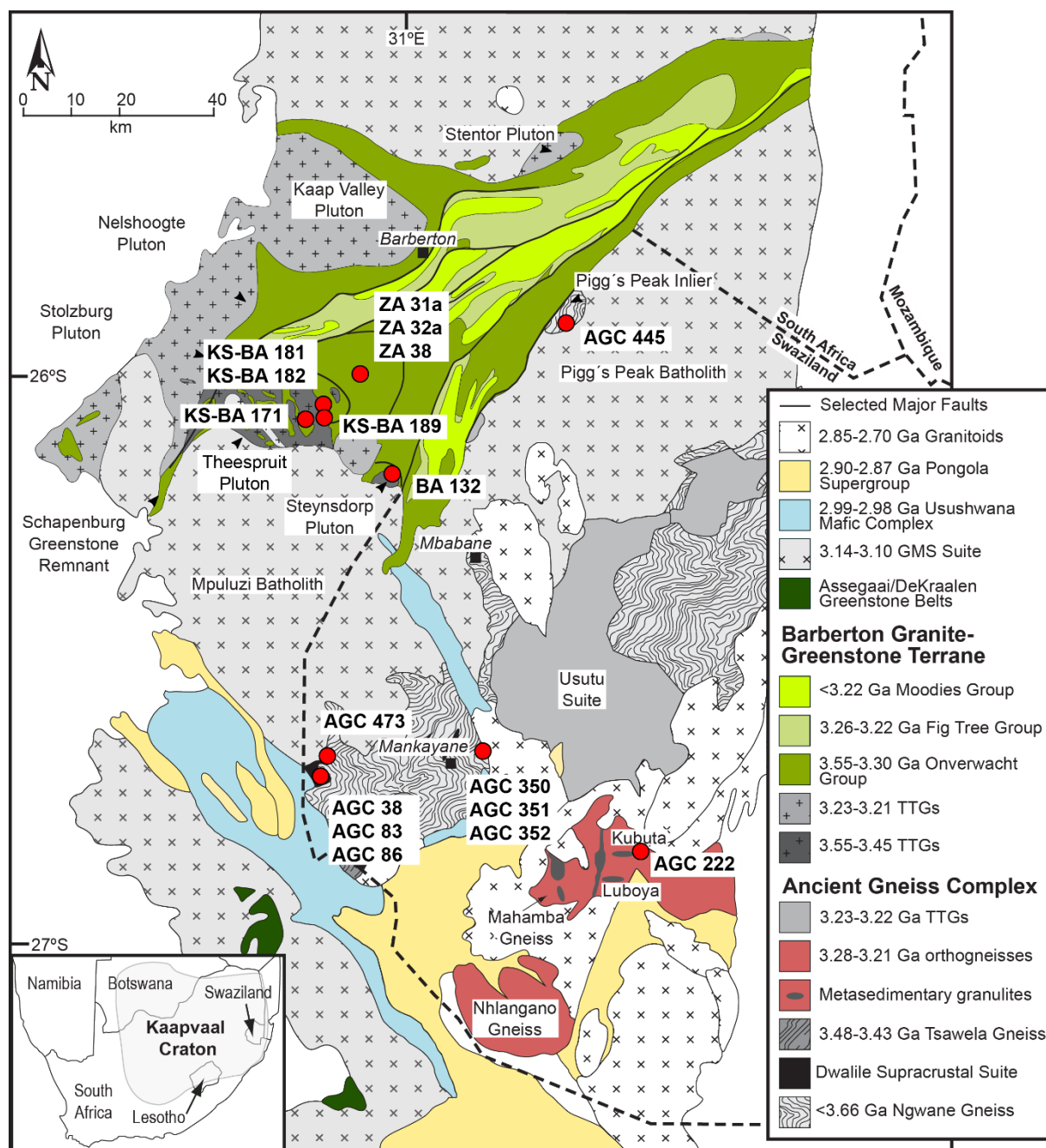


Fig. S13: Simplified geological map of the Kaapvaal Craton, Southern Africa, showing the sample localities covered in this study. The map is taken from Ref. 15 and modified after Ref. 113.

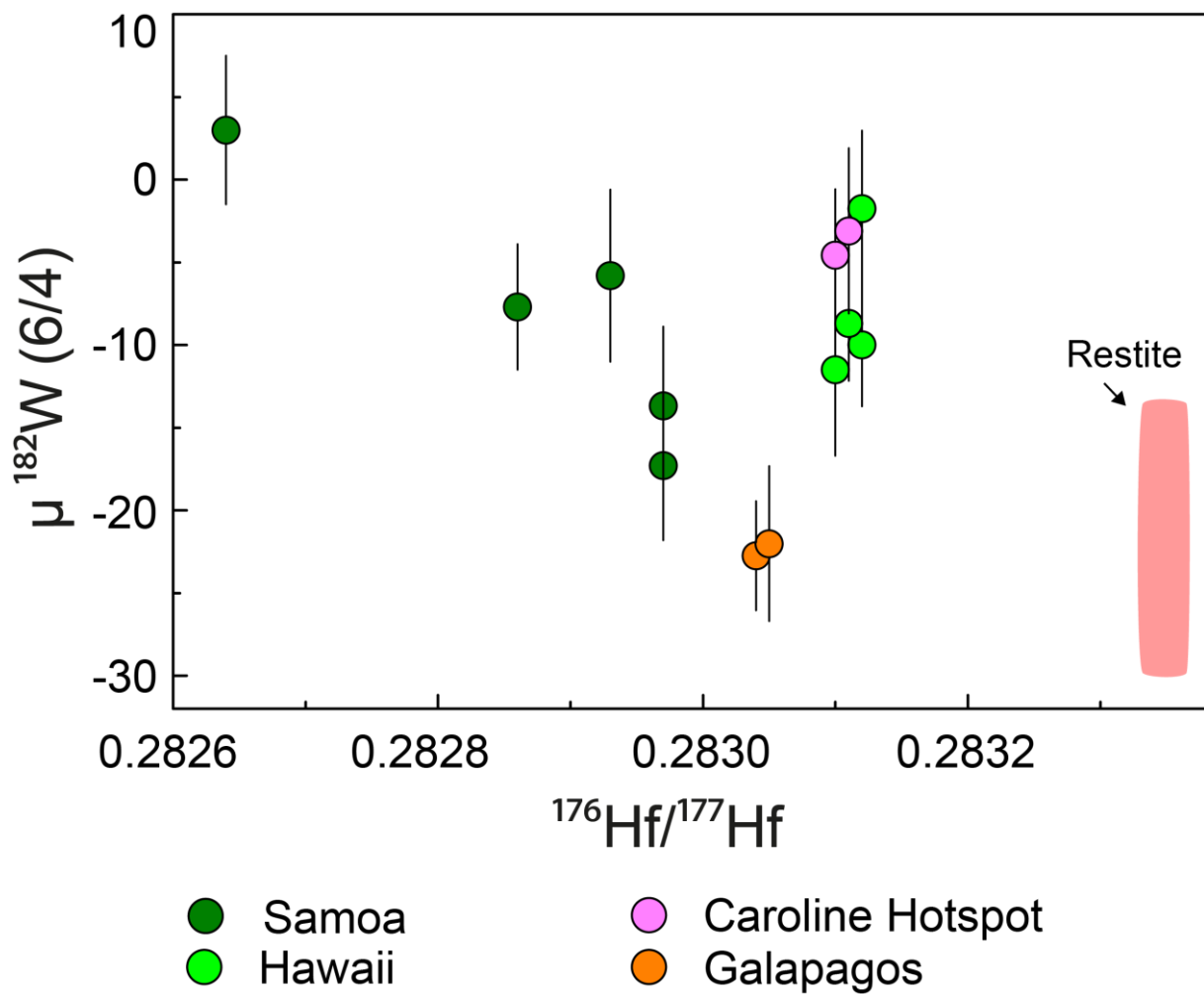


Fig. S14: Compilation of ^{182}W and ^{176}Hf isotope compositions for modern OIBs. Data were compiled from recent studies(8, 59) and references therein. As for $\mu^{182}\text{W}$ vs. $^{143}\text{Nd}/^{144}\text{Nd}$ (see Fig. 5) the global compilation for modern OIBs displays a similar pattern for $\mu^{182}\text{W}$ vs. $^{176}\text{Hf}/^{177}\text{Hf}$, although only less constrained by the limited ^{176}Hf isotope data available. Also shown is the present ^{182}W and ^{143}Nd isotope composition calculated for restites that remained after prolonged TTG formation (4.35 – 4.25 Ga) via partial anatexis of a mafic protocrust that formed between 40 and 50 Ma after solar system formation (pink array).

1824

1825 **References SI Appendix**

- 1826 103. J. E. Hoffmann, A. Kröner, “Early Archean crustal evolution in southern Africa -
1827 an updated record of the Ancient Gneiss Complex of Swaziland” in *Earth’s*
1828 *Oldest Rocks*, 2nd Ed., M. J. Van Kranendonk, Ed. (Elsevier, 2019), pp. 553–
1829 567.
- 1830 104. A. Kröner, W. Compston, I. S. Williams, Growth of early Archaean crust in the
1831 Ancient Gneiss Complex of Swaziland as revealed by single zircon dating.
1832 *Tectonophysics* **161**, 271–298 (1989).
- 1833 105. A. C. Wilson, 1:250,000 Geological Map of Swaziland. *Geol. Surv. Mines Dep.*
1834 *Mbabane, Swazil.* (1982).
- 1835 106. B. Schoene, M. J. de Wit, S. A. Bowring, Mesoarchean assembly and
1836 stabilization of the eastern Kaapvaal craton: A structural-thermochronological
1837 perspective. *Tectonics* **27**, 1–27 (2008).
- 1838 107. A. Kröner, J. I. Wendt, C. Milisenda, W. Compston, R. Maphalala, “Zircon
1839 geochronology and Nd isotopic systematics of the Ancient Gneiss Complex,
1840 Swaziland, and implications for crustal evolution” in *The Ancient Gneiss*
1841 *Complex: Overview Papers and Guidebook for Excursion*, Bulletin 1, A. Kröner,
1842 Ed. (Swaziland Geological Survey and Mines Department, 1993), pp. 15–37.
- 1843 108. A. Kröner, Chapter 5.2 The Ancient Gneiss Complex of Swaziland and
1844 Environs: Record of Early Archean Crustal Evolution in Southern Africa. *Dev.*
1845 *Precambrian Geol.* **15**, 465–480 (2007).
- 1846 109. M. P. A. Jackson, “Archean structural styles in the Ancient Gneiss Complex of
1847 Swaziland, South Africa” in *Precambrian Tectonics Illustrated*, A. Kröner, R.
1848 Greiling, Eds. (Schweizerbart’sche Verlagsbuchhandlung, 1984), pp. 1–18.
- 1849 110. A. Kröner, A. Tegtmeier, Gneiss-greenstone relationships in the Ancient
1850 Gneiss Complex of southwestern Swaziland, southern Africa, and implications
1851 for early crustal evolution. *Precambrian Res.* **67**, 109–139 (1994).
- 1852 111. D. R. Hunter, F. Barker, H. T. Millard, Geochemical investigation of Archaean
1853 Bimodal and Dwalile metamorphic suites, Ancient Gneiss Complex, Swaziland.
1854 *Precambrian Res.* **24**, 131–155 (1984).
- 1855 112. A. Kröner, *et al.*, “Archaean Crystalline Rocks of the Eastern Kaapvaal Craton”
1856 in *The Archaean Geology of the Kaapvaal Craton, Southern Africa, Regional*
1857 *Geology Reviews*, A. Kröner, A. Hofmann, Eds. (Springer Nature Switzerland
1858 AG, 2019), pp. 1–32.
- 1859 113. V. van Schijndel, G. Stevens, A. Zeh, D. Frei, C. Lana, Zircon geochronology
1860 and Hf isotopes of the Dwalile Supracrustal Suite, Ancient Gneiss Complex,
1861 Swaziland: Insights into the diversity of Palaeoarchaeoan source rocks,
1862 depositional and metamorphic ages. *Precambrian Res.* **295**, 48–66 (2017).
- 1863 114. J. E. Hoffmann, *et al.*, Source composition, fractional crystallization and magma
1864 mixing processes in the 3.48-3.43 Ga Tsawela tonalite suite (Ancient Gneiss
1865 Complex, Swaziland) - Implications for Palaeoarchaeoan geodynamics.
1866 *Precambrian Res.* **276**, 43–66 (2016).

- 1867 115. S. B. Mukasa, A. H. Wilson, K. R. Young, Geochronological constraints on the
1868 magmatic and tectonic development of the Pongola Supergroup (Central
1869 Region), South Africa. *Precambrian Res.* **224**, 268–286 (2013).
- 1870 116. A. Kröner, *et al.*, High-temperature metamorphism and crustal melting at ca.
1871 3.2 Ga in the eastern Kaapvaal craton, southern Africa. *Precambrian Res.* **317**,
1872 101–116 (2018).
- 1873 117. J. F. Moyen, G. Stevens, A. F. M. Kisters, R. W. Belcher, B. Lemirre, “TTG
1874 plutons of the Barberton granitoid-greenstone terrain, southern Africa” in
1875 *Earth’s Oldest Rocks*, 2nd Ed., M. J. Van Kranendonk, V. C. Bennett, J. E.
1876 Hoffmann, Eds. (Elsevier, 2018), pp. 615–653.
- 1877 118. N. Suhr, J. E. Hoffmann, A. Kröner, S. Schröder, Archaean granulite-facies
1878 paragneisses from central Swaziland: Inferences on Palaeoarchaeon crustal
1879 reworking and a complex metamorphic history. *J. Geol. Soc. London.* **172**,
1880 139–152 (2014).
- 1881 119. G. R. Byerly, D. R. Lowe, C. Heubeck, “Geologic evolution of the Barberton
1882 Greenstone Belt - A unique record of crustal development, surface processes,
1883 and early life 3.55 - 3.20 Ga” in *Earth’s Oldest Rocks*, 2nd Ed., M. J. Van
1884 Kranendonk, V. C. Bennett, J. E. Hoffmann, Eds. (Elsevier, 2018), pp. 569–
1885 613.
- 1886 120. R. A. Armstrong, W. Compston, M. J. de Wit, I. S. Williams, The stratigraphy of
1887 the 3.5-3.2 Ga Barberton Greenstone Belt revisited: a single zircon ion
1888 microprobe study. *Earth Planet. Sci. Lett.* **101**, 90–106 (1990).
- 1889 121. A. Kröner, *et al.*, Chronology of the oldest supracrustal sequences in the
1890 Palaeoarchaeon Barberton Greenstone Belt, South Africa and Swaziland.
1891 *Precambrian Res.* **279**, 123–143 (2016).
- 1892 122. J. C. Dann, The 3.5 Ga Komati Formation, Barberton Greenstone Belt, South
1893 Africa, Part I: New maps and magmatic architecture. *South African J. Geol.*
1894 **103**, 47–68 (2000).
- 1895 123. C. R. Anhaeusser, Magmatic and structural characteristics of the ca. 3440 ma
1896 theespruit pluton, barberton mountain land, South Africa. *Am. J. Sci.* **310**,
1897 1136–1167 (2010).
- 1898 124. M. J. Van Kranendonk, A. Kröner, J. E. Hoffman, T. Nagel, C. R. Anhaeusser,
1899 Just another drip: Re-analysis of a proposed mesoarchean suture from the
1900 Barberton mountain land, South Africa. *Precambrian Res.* **254**, 19–35 (2014).
- 1901 125. N. T. Arndt, *et al.*, Scientific drilling in the Barberton Greenstone Belt.
1902 *Geobulletin* **53**, 17–18 (2010).
- 1903 126. K. R. Bermingham, R. J. Walker, The ruthenium isotopic composition of the
1904 oceanic mantle. *Earth Planet. Sci. Lett.* **474**, 466–473 (2017).
- 1905 127. M. R. Savina, *et al.*, Extinct Technetium in Silicon Carbide Stardust Grains:
1906 Implications for Stellar Nucleosynthesis. *Science (80-.)*. **303**, 649–652 (2004).
- 1907 128. J. Blichert-Toft, N. T. Arndt, Hf isotope compositions of komatiites. *Earth*
1908 *Planet. Sci. Lett.* **171**, 439–451 (1999).
- 1909 129. Y. Lahaye, *et al.*, The influence of alteration on the trace-element and Nd

- 1910 isotopic compositions of komatiites. *Chem. Geol.* **126**, 43–64 (1995).
- 1911 130. A. Kröner, *et al.*, Generation of early Archaean felsic greenstone volcanic rocks
1912 through crustal melting in the Kaapvaal, craton, southern Africa. *Earth Planet.*
1913 *Sci. Lett.* **381**, 188–197 (2013).
- 1914 131. J. Blichert-Toft, N. T. Arndt, G. Gruau, Hf isotopic measurements on Barberton
1915 komatiites: Effects of incomplete sample dissolution and importance for primary
1916 and secondary magmatic signatures. *Chem. Geol.* **207**, 261–275 (2004).
- 1917 132. C. Lécuyer, G. Gruau, C. R. Anhaeusser, S. Fourcade, The origin of fluids and
1918 the effects of metamorphism on the primary chemical compositions of
1919 Barberton komatiites: New evidence from geochemical (REE) and isotopic (Nd,
1920 O, H, ³⁹Ar/⁴⁰Ar) data. *Geochim. Cosmochim. Acta* **58**, 969–984 (1994).
- 1921